

GPR DATA PROCESSING FOR REINFORCED CONCRETE BRIDGE DECKS

A Thesis
Presented to
The Academic Faculty

by

Xiangmin Wei

In Partial Fulfillment
of the Requirements for the Degree
Doctor of Philosophy in the
School of Electrical and Computer Engineering

Georgia Institute of Technology
December 2014

Copyright © 2014 by Xiangmin Wei

GPR DATA PROCESSING FOR REINFORCED CONCRETE BRIDGE DECKS

Approved by:

Professor Ying Zhang, Advisor
School of Electrical and Computer
Engineering
Georgia Institute of Technology

Professor Waymond R. Scott
School of Electrical and Computer
Engineering
Georgia Institute of Technology

Professor Ghassan AlRegib
School of Electrical and Computer
Engineering
Georgia Institute of Technology

Professor Andrew F. Peterson
School of Electrical and Computer
Engineering
Georgia Institute of Technology

Professor Yang Wang
School of Civil and Environmental
Engineering
Georgia Institute of Technology

Date Approved: 10 November 2014

*To myself, my family,
my advisor, and my friends*

ACKNOWLEDGEMENTS

First, I would like to express my gratitude to my advisor, Dr. Ying Zhang, for her financial support and guidance throughout my Ph.D. program. I believe without her kindness, patience, and knowledge, I cannot survive my Ph.D. journey. You are an awesome advisor, and for this, I thank you.

Second, I am very grateful to Dr. Waymond R. Scott for his selfless guidance even though I am not one of his students. I am very impressed by his expertise on ground penetrating radar.

Third, I also owe my gratitude to all members of my dissertation committee: Dr. Waymond R. Scott, Dr. Ghassan AlRegib, Dr. Andrew F. Peterson, and Dr. Yang Wang for services and valuable suggestions on the work done in this dissertation.

Fourth, I would also like to thank my fellow lab members who provided great collaboration and assistance during my study. You have made my long journey much more cheerful.

Finally, I am greatly indebted to my family and friends, especially my parents, for their love and support.

TABLE OF CONTENTS

DEDICATION	iii
ACKNOWLEDGEMENTS	iv
LIST OF FIGURES	vii
SUMMARY	x
I INTRODUCTION	1
1.1 Background and Motivation	1
1.1.1 Autofocusing	2
1.1.2 Interference Removal	4
1.1.3 CS-Based Migration	7
1.2 Dissertation Outline	9
II AUTOFOCUSING	10
2.1 Proposed Approach	10
2.1.1 Stolt F-K Migration	10
2.1.2 Autofocusing Metrics	13
2.2 Simulation Study	15
2.2.1 Simulation Setup	15
2.2.2 Preprocessing	17
2.2.3 Results and Discussions	18
2.3 Experimental Study	27
2.3.1 Experimental Setup	27
2.3.2 Results and Discussions	27
2.4 Summary	36
III INTERFERENCE REMOVAL	37
3.1 Proposed Approach	37
3.1.1 Theory of F-K Filtering	39
3.1.2 Dip Relaxation	41

3.2	Simulation Demonstration	41
3.3	Experimental and Field Study	44
3.3.1	Data Collection	44
3.3.2	Results and Discussions	46
3.4	Summary	50
IV	MODIFIED CS-BASED MIGRATION	51
4.1	Theory of CS-Based Migration	51
4.2	Waveform Distortion Mechanisms	53
4.3	Simulation Study	55
4.3.1	Direct Waves	55
4.3.2	Waveform Distortion	59
4.3.3	Comparative Amplitude Preservation	60
4.3.4	Uniform Downsampling	64
4.4	Experimental Demonstration	69
4.5	Summary	71
V	CONCLUSION	72
5.1	Dissertation Contribution	72
5.2	Future Work	73
	REFERENCES	74
	VITA	82

LIST OF FIGURES

1	The cross section of the simulated RC bridge deck.	16
2	The original 2D GPR profile.	17
3	The preprocessed GPR profile.	18
4	Migrated profiles with (a) a higher velocity, (b) a lower velocity, and (c) the real velocity.	19
5	Metric performance for the clean GPR profile.	20
6	GPR profile with white noise (SNR=-50).	21
7	Metric performance for (a) SNR=-30dB, (b) SNR=-55dB, and (c) SNR=-60dB.	22
8	GPR profile polluted with salt and pepper noise.	23
9	Metric performance for GPR profile with salt and pepper noise.	23
10	Metric performance for data with the aperture width of (a) 100 traces and (b) 30 traces.	25
11	Metric performance for data with the cross rebar reflections and (a) SNR = -30dB and (b) SNR = -55dB.	26
12	The bird's-eye view of the fabricated RC bridge deck.	29
13	(a) The original profile and (b) the preprocessed profile of the GPR data collected along the vertical line at 3.65 m (12.00 ft.) along the horizontal axis.	30
14	The migrated GPR profile with a constant velocity.	31
15	Metric performance for the leftmost rebar.	31
16	(a) The optimized RDP distribution and (b) the corresponding migrated GPR profile.	32
17	(a) The original profile and (b) the preprocessed profile of the GPR data collected along the vertical line at 3.72 m (12.25 ft.) along the horizontal axis.	34
18	Metric performance for the rightmost rebar (a) with the full aperture and (b) with 30 traces less.	35
19	Simulated GPR profiles with (a) only direct waves in the T-X domain and (b) in the F-K domain; (c) only target signals in the T-X domain and (d) in the F-K domain	43

20	Simulated GPR profiles after (a) F-K filtering and (a) BS.	44
21	The original GPR profile collected from the experimental specimen. .	45
22	Route 15 bridge over I-66 in Haymarket, Virginia.	45
23	The original GPR profile collected from the real bridge deck.	46
24	The experimental GPR profiles after (a) BS, and F-K filtering with (b) adequate dip relaxation, (c) no dip relaxation, (d) non-adequate dip relaxation.	48
25	The field GPR profiles after (a) BS, and F-K filtering with (b) adequate dip relaxation, (c) no dip relaxation, and (d) non-adequate dip relaxation.	49
26	Performance comparison of HOT for preprocessed data after BS and F-K filtering.	50
27	Simulated GPR profiles of (a) the original data and (b) the preprocessed data.	57
28	Results of (a) CS-based migration with a low regularization parameter, (b) CS-based migration with a high regularization parameter, and (c) F-K migration on the original GPR data.	58
29	Results of (a) CS-based migration and (b) F-K migration on the preprocessed GPR data.	59
30	Rebar reflection and the best matching dictionary element.	60
31	CS-based migration with (a) the previous model and (b) the modified model.	60
32	(a) The original GPR profile and (b) preprocessed GPR profile for multiple rebars.	62
33	(a) CS-based migration results with a high regularization parameter and (b) with a low regularization parameter, and (c) F-K migration results for the preprocessed GPR profile with multiple rebars.	63
34	The results of the proposed amplitude reservation method for multiple rebars when the rebar spacing is integral multiples of the scan step. .	64
35	The results of the proposed amplitude reservation method for multiple rebars when the rebar spacing is not integral multiples of the scan step.	64
36	The downsampled GPR profile for temporal downsampling rate of 70.	66
37	(a) CS-based migration and (b) F-K migration results for temporal downsampling rate of 70.	66
38	POR with various temporal downsampling rates.	67

39	The downsampled GPR profile for spatial downsampling rate of 6. . .	68
40	(a) CS-based migration and F-K migration results for spatial down- sampling rate of 6.	68
41	ROR with various spatial downsampling rates.	69
42	The results of the proposed amplitude reservation method for multiple rebars when the rebar spacing is not integral multiples of the scan step (down sampling rate is 2).	69
43	Original GPR profile and the preprocessed GPR profile for the exper- imental data.	70
44	Segmented GPR profile for the leftmost rebar.	70
45	Results of (a) CS-based migration and (b) F-K migration.	71

SUMMARY

Ground penetrating radar (GPR) has been successfully applied in multiple areas for shallow subsurface probing and has been recently recognized as a primary investigation tool for the non-destructive evaluation of reinforced concrete (RC) bridge decks. In this thesis, several aspects of GPR data processing for RC bridge decks are studied. First, autofocus techniques are proposed to replace the previous expensive and unreliable human visual inspections during the iterative migration process for the estimation of the velocity/dielectric permittivity distribution from GPR data. The investigation of the metric performance is conducted on simulation data and the conclusions are validated by experimental data. Second, F-K filtering with dip relaxation is proposed for interference removal that is important for both imaging and the performance of post-processing techniques including autofocus techniques and CS-based migration studied in this thesis. The targeted interferes here are direct waves and cross rebar reflections. The introduced dip relaxation is for accommodating surface roughness and medium inhomogeneity. The basic principle of the proposed method is demonstrated using simulation data and the effectiveness is validated by experimental and field data. Third, the newly developed CS-based migration is modified and evaluated on GPR data from RC bridge decks. A more accurate model by accounting for impulse waveform distortion that leads to less modeling errors is proposed. The impact of the selection of the regularization parameter on the comparative amplitude reservation and the imaging performance is also investigated, and a simple approach to preserve the comparative amplitude information while still maintaining a clear image is proposed. Moreover, the potential of initially sampling the time-spatial data with uniform sampling rates lower than that required by traditional

migration methods is studied. The evaluation is made on simulation data and then follows an experimental demonstration.

CHAPTER I

INTRODUCTION

1.1 Background and Motivation

More than a quarter of bridges in the U.S. are reported as structurally deficient or functionally obsolete [1]. The network-level evaluation and the maintenance under a tight budget are of significant importance. To reinforced concrete (RC) bridge deck engineers and researchers, the deterioration phenomena of highest concern are rebar corrosion, deck delamination, vertical cracking, and concrete degradation. Although coring is the most accurate way to evaluate the bridge quality, its usage is greatly hindered by its destructive nature. Non-destruction evaluation (NDE) techniques, such as impact echo [85][78], chain dragging and hammer sounding, ultrasonic pulse echo, ultrasonic surface waves, impulse response, ground-penetrating radar (GPR), half-cell potential, galvanostatic pulse measurement, electrical resistivity and infrared thermography, become available and each of them has its own advantages and disadvantages [33].

Among various NDE techniques, GPR has been recognized by the Federal Highway Administration (FHWA) and many state transportation departments as a primary investigative tool for the evaluation of RC bridge decks [9]. The benefits include fine resolution, fast data acquisition speed, safe and weather-independent operations [16], high repeatability, no need of asphalt removal, deck thickness estimation, rebar localization, rebar diameter estimation, and area estimation of corrosion-induced damages.

The primary information extracted from the GPR data collected from RC bridge decks are the rebar locations and the attenuation map. Precisely determining the

rebar positions during the renovation of the bridge surface layer can avoid damages to the rebars when holes are drilled into the concrete body to anchor the new layer, and hence ensure the safety of the workers and the stability of the bridge [42]. The attenuation map is the most popular network-level interpretation method to evaluate the health condition of bridge decks and it is produced by plotting the amplitudes of the migrated rebar reflections after depth correction on a 2D figure. The attenuation map is usually smoothed using various interpolation methods, such as B-spline interpolation or interpolation based on mixtures of gaussian process models [52][51]. Areas with comparatively low signal strength, indicating high loss, are generally considered as an indication of serious concrete degradation or rebar corrosion [10].

GPR has been applied for shallow subsurface imaging in multiple areas such as archaeology [86], civil engineering [76], forensics [55], geophysics [87], unexpected ordnance (UXO) detection [20], and utility detection [23], due to its sensitivity to variations of electrical permittivity, electrical conductivity, and magnetic permeability [83, 21]. For the application of RC bridge deck evaluation, there still exist multiple obstacles. This thesis is aimed to solve a small amount of the remaining problems and explore new techniques, which will be introduced in the following part of this chapter.

1.1.1 Autofocusing

Surface collected GPR profiles sometimes deviate from the real subsurface structures. For a point-like object, a hyperbolic shape is formed on the radargram as a result of the wide antenna beamwidth and the two-way travel (TWT) time variations caused by the antenna movement along the measurement line. In order to accurately interpret the GPR profiles, a back-propagation process needs to be performed to collapse the diffracted signals back into its true physical shape and position [38]. The back-propagation process is also called migration. The migration techniques are widely

studied in the seismic field due to the momentum of hydrocarbon exploration.

The most important input for migration techniques is the subsurface medium velocity distribution, which is equivalent to the relative dielectric permittivity (RDP) distribution for low loss medium. However, this information is usually not available beforehand and itself is also valuable for the RC bridge deck diagnosis. Due to its importance, velocity analysis has been long discussed in the seismic field, but the techniques developed can be difficult to be adapted to the application of RC bridge decks directly. The traditional approaches to obtain the information of the medium velocity distribution include point-to-point coring, time domain reflectometry (TDR) measurements [66][39], and multi-offset data analysis [15]. The first two methods can be destructive, and require extra systems and measurements. Multi-offset data analysis uses techniques such as normal moveout (NMO) [56] velocity analysis and residual moveout (RMO) velocity analysis [15]. The setup can be common midpoint, common transmitter, or common receiver. Although velocity analysis based on multifold data has been adopted by some GPR systems, it is not favored by RC bridge deck inspections due to the prolonged data acquisition time that will lead to longer traffic interruption. Besides, the most commonly used NMO velocity analysis has additional requirements such as clear reflecting layers [5]. Moreover, the most popular GPR system for the RC bridge deck inspection is built with common-offset antennas due to its simple design and low cost [21].

For the common-offset GPR systems, the local medium velocity can be estimated using the reflections from the cooperative targets that can be pre-built in if none exist in the subsurface. For RC bridge deck inspection, the rebars are the natural cooperative objects and the density is generally high enough for the optimized decision making under a tight budget. There are several approaches for velocity determination using cooperative targets, such as hyperbola shape analysis-based method,

Hough transform-based method, and migration-based method. The first two methods are reported to generate less accurate results or require extra prior information as compared to the migration-based method [64]. The decision-making process for the migration-based method is mostly based on visual inspections of an iterative trial-and-error process, which combines direction change of the migration curves and focus points [13]. The discretized permittivity values in a reasonable range are used to generate a series of migrated GPR profiles and then visual inspections are performed to pick the velocity that produces the best focused image. Two problems arise from this process. One is the high computational cost from the iterative process. There are already researchers working on it and it will not be the focus of this thesis. For example, a time image-wave remigration is developed and applied on zero-offset GPR data to generate a batch of migrated radargrams using various migration velocities with less computational cost [54]. The other problem is the human visual inspections required in this process. Human visual inspections are usually subjective and expensive, and can even fail when the signal-to-noise ratio (SNR) is low. Therefore, accurate, robust, and sensitive autofocusing techniques replacing visual inspections are needed. Hopefully, it can also generate reasonable results in situations where visual inspections fail.

1.1.2 Interference Removal

Interference removal is an important process for imaging purposes. In addition, the evaluation of the autofocusing techniques indicate that strong direct waves (antenna crosstalk and ground bounce) and cross rebar reflections can substantially deteriorate the performance of the postprocessing techniques. It is essential to effectively remove the interferences before further processing the GPR data collected from RC bridge decks.

Direct wave removal from GPR data has been long studied and various methods

have been proposed and implemented. Conventional approaches include background average removal, time-gating, and scale and shift. However, those techniques fail when the surface is rough or when the target signals are mixed with the direct waves [27]. For RC bridge decks, the top rebar mat are usually located at a shallow depth, e.g., 2.5 in., and hence the rebar reflections from this layer is usually overlapped with direct waves. In addition, the surface roughness of the RC bridge deck, especially asphalt overlaid decks, sometimes cannot be neglected. In these cases, the conventional approaches cannot provide high-quality preprocessed GPR profiles for both imaging and further processing. Unconventional direct wave removal methods explore both hardware and advanced software solutions. There are numerous research papers working on this topic and each has its own suitable occasions and restrictions. Hardware solutions include differential GPR systems [60], GPR systems with transmitter-receiver-transmitter configuration (TRT) [36][37], and GPR systems with transmitters at the Brewster angle [39]. The Differential GPR system records the differences of two receivers located at the same distance from the underground surface and symmetric to the transmitter. The TRT GPR system shares similar setup as the differential GPR system. It feeds the transmitters out-of-phase sources to create a symmetric plane in the middle. Both types of GPR systems require homogeneous subsurface and uniform air-subsurface interface, and may cause the filtering of useful signals for targets of low spatial variations. For the third GPR configuration, setting the transmitter at the Brewster angle is unpractical for field scans as it requires medium homogeneity and the prior information of medium permittivity. Moreover, this method is only effective in removing ground bounce and the suppression of the crosstalk between antennas requires additional processing. Advanced software solutions can be generally classified into parameterization/statistics-based methods and filtering-based methods [67]. The main drawback of parameterization/statistics-based methods is that it requires reference data and the performance strongly depends on

the clutter model and the assumptions for parameter estimation [84, 24, 70]. Filtering methods include decomposition using component separation/subspace projection (ICA/PCA/Eigenvalues/SVD) [67, 44, 72], wavelet filtering [63], Kalman filtering [71], and frequency-wavenumber (F-K) filtering [39]. Component separation is based on the assumption that the interferences are the leading component, which may not always hold. In [67], the average removal and the subspace projection methods are compared with the entropy-based time-gating approach. The authors demonstrate that the average removal and the subspace projection methods provide very similar results, and both methods return images with larger clutter residues compared with the entropy-based time-gating approach. Although the entropy-based time-gating approach provides better results, it is not suitable for our application. When the clutter and the rebar reflections are heavily mixed in our application, zeroing out points corresponding to the clutter will result in a significant loss of target signals. In addition, a windowing along the scan line direction may erase a large part of the gathered target signals, which contains information that is important for the further processing of the GPR data from RC bridge decks. In [63], the 2D wavelet transform methods are tested on the GPR profiles collected from the underground buried with metal/plastic tubes and the test data are similar to the GPR data collected from RC bridge decks, but in a much simpler scenario that the underground surface is flatter, the medium is more homogeneous and the interferences are less overlapped with the target signals. Although a large amount of the direct waves are removed by the wavelet transform-based methods, the clutter residues are still not trivial. Kalman filter in [71] requires reference data, which are not always available. The adopted method in this thesis is based on F-K filtering and it will be presented in Chapter III.

On the other hand, cross rebar reflections are considered as useful information for 3D GPR imaging and its removal is rarely discussed in the literature. However, the cross rebar reflection removal is necessary for the autofocusing process of the 2D

GPR profile analysis as well as the newly developed CS-based migration when the GPR scanning line gets close to a cross rebar. Additionally, the removal of cross rebar signals can also improve the accuracy of the attenuation map [10]. For the GPR data from RC bridge decks, cross rebar reflection has two features that make it difficult to be eliminated by the existing methods developed for the direct wave removal. First, the heterogeneity of concrete medium contributes to the uneven cross rebar images in the profiles. Second, nearby cross rebar signals are usually overlapped with the rebar signals under investigation as rebars from both directions are from the same rebar mat and they are almost at the same depth. Therefore, to explore new interference removal techniques handling difficult situations is beneficial for both imaging and postprocessing.

1.1.3 CS-Based Migration

Recent progress in the compressive sensing (CS) theory has provided an alternative method for the migration of sparse GPR signals. In CS theory, an array of unknowns, x , of length N and sparsity of K , can be reconstructed exactly with high probability from $O(K \log N)$ CS measurements, y ($y = Ax$, in the form of randomized projections), by solving l_1 convex optimization problems [22, 17, 8]. This concept has later been utilized in the application of GPR for landmine detection [35][34]. The sparsity here means the number of the user-defined grids of the total imaged subsurface is much larger than the number of target grids. The assumptions are as follows. The targets are sparse and point-like at discrete locations, the targets do not interact with each other and the superposition is valid, the wave propagation obey ray theory, and the subsurface medium is homogeneous. Compared to traditional imaging methods, less cluttered high-resolution images are obtained using a small amount of CS measurements for the application of landmine detection. Similar ideas are followed by [40] for through-the-wall imaging.

The CS-based migration is attempted and modified in this thesis for the application of GPR data from RC bridge decks. First, a more accurate model needs to be built by embracing waveform distortion mechanisms. In the previous model, the impulse distortion that may be caused by factors such as antennas, dispersive mediums, or reflective objects are not taken into consideration. As real data have shown severe distortion of the impulse wavelets reflected from subsurface objects for the GPR probing of RC structure and many other applications, modeling errors will be increased if the distortion is neglected. This problem will be even more important when the original images need to be recovered. Second, an approach to obtain clear images while still preserving the comparative amplitude information needs to be developed. The investigation using various regularization parameters shows that a high value for the regularization parameter is able to preserve the comparative amplitude information, but the image can be heavily blurred; a low value for the regularization parameter achieves the opposite performance. It is hardly possible to achieve sparse and clear GPR images while still preserving the comparative amplitude information when the whole B-scan with multiple targets (rebars) is processed by CS-based migration. As the major tool to perform the network-level bridge deck inspection using GPR is the attenuation map, which is made based on the amplitude of the rebar reflections, it will be more practical for CS-based migration to provide clear GPR images while still preserve the comparative amplitude information. Third, direct sampling using uniform sampling rates less than the traditional migration methods is worth an investigation for the purpose of less sampled data and less data acquisition time. Although GPR is much faster compared to other NDE techniques for RC bridge decks, it still requires traffic interruption for most cases. One of the major factors that hinders the increase of the data acquisition speed of GPR systems is that traditional migration techniques require fine spatial sampling and Nyquist-rate time samples of the received data. Most CS measurements require difficult or complicated extra hardware and less

CS measurements are generally not equivalent to less direct measurements. Among various CS measuring methods, random sampling along the spatial domain has the potential to decrease the data acquisition time, but the recovery of the uniformly distributed targets can be risky. An effort is worth to be made on revealing the potential of CS-based migration using smaller uniform sampling rates and larger scan intervals than that required by the traditional migration techniques. In both directions, it can help reduce the size of directly measured data. A larger uniform scan interval will lead to a faster data acquisition speed.

1.2 Dissertation Outline

The remaining part of this dissertation is organized as follows. Chapter II introduces multiple autofocusing techniques and evaluate the performances with respect to random noise, synthetic aperture width, and cross rebar reflection interferences using simulation data and the conclusions are also validated on experimental data. Chapter III presents an F-K filtering with dip relaxation for accommodating the uneven line-like structures of the interferences that can be caused by surface roughness and medium inhomogeneity. The principle is illustrated using simulation data. The effectiveness is also evaluated by comparing the results with that of the standard direct wave removal method on both experimental and field data. Chapter IV presents a modified CS-based migration by accurately modeling the waveform distortion mechanisms, an approach to obtain clear GPR images while still preserve the comparative amplitude information, and performance evaluation of uniform downsampling. The study is based on simulation data and then follows an experimental demonstration. Chapter V concludes the thesis.

CHAPTER II

AUTOFOCUSING

2.1 Proposed Approach

In this thesis, the proposed approach is to select candidate autofocus metrics from other fields, such as optical and synthetic aperture radar (SAR) imaging, to replace the previous visual inspections during the iterative migration process. The selected autofocus metrics are carefully studied first using simulation data for evaluating the effects of possible factors that might deteriorate the performance of the metrics on GPR data from RC bridge decks, and then the effectiveness is demonstrated by experimental data. Consistent conclusions can be drawn from both simulation and experimental study. As Stolt F-K migration is adopted as a traditional migration technique throughout this thesis, a brief introduction is first given in the following subsection.

2.1.1 Stolt F-K Migration

A large library of migration techniques has come into existence since the pioneer work of Jon F. Claerbout with the development of fast computers [19]. The classical algorithms include Kirchhoff integral method [62], finite-difference migration [29], Stolt F-K migration [68], Gazdag phase-shift migration [30], and their cascaded or hybrid versions [13]. Among them, Stolt migration, first brought up in the seismic field, is reported to be accurate and computational efficient. F-K migration or its variations have been adopted by satellite SAR image processing and widely utilized for GPR data processing [58]. There also exist other newly developed migration techniques that are not based on scalar wave equations, such as vertical offset filtering (VOF) [11]. VOF requires collecting GPR traces repeatedly at the same spot with

the antenna lifted at different predetermined heights, which makes it unsuitable for our application by hindering the data acquisition speed and complicating the GPR system. The evaluation of the autofocusing metrics in this thesis are based on the results from Stolt F-K migration, but the conclusion drawn can be readily generalized to other back-prorogation techniques. The theoretic deduction of Stolt F-K migration is briefly introduced as follows.

Here we consider the surface collected data as a 2D matrix $s(x, z = 0, t)$ with x being the Cartesian coordinate along the scanning axis, z the depth, and t the sampling time. Applying the 2D Fourier transform with respect to x to the horizontal spatial frequency, k_x , and t to the angular frequency, ω , yields an unfocused F-K domain dataset:

$$S(k_x, z = 0, \omega) = \iint s(x, z = 0, t) e^{-jk_x x} e^{-j\omega t} dx dt. \quad (1)$$

Accounting only upward coming waves, and introducing the wavenumber along the depth direction, k_z , the wavefront in the F-K domain at depth, z , can be acquired by

$$S(k_z, z, \omega) = S(k_x, z = 0, \omega) \cdot e^{jk_z z}. \quad (2)$$

Then a 2D IFFT is implemented to transform the data back from the F-K domain and the trick is done during this process:

$$s(x, z, t) = \frac{1}{4\pi^2} \iint S(k_x, z, \omega) e^{jk_x x} e^{j\omega t} dk_x d\omega. \quad (3)$$

The migrated data will be the inverse Fourier transforms at $t = 0$ as

$$s(x, z, t = 0) = \frac{1}{4\pi^2} \iint S(k_x, z = 0, \omega) e^{jk_x x} e^{jk_z z} dk_x d\omega. \quad (4)$$

According to the scalar wave theory in a homogeneous medium,

$$\nabla^2 u + \frac{4}{v^2} \cdot \frac{\partial^2 u}{\partial t^2} = 0, \quad (5)$$

where v is the propagation velocity ($v = c/\sqrt{\varepsilon_r}$) with ε_r the relative dielectric constant, c the speed of light in vacuum). After applying Fourier transform and defining the total wavenumber vector, k , we can obtain

$$k^2 - \left[\frac{2\omega}{v} \right]^2 = k_x^2 + k_z^2 - \left[\frac{2\omega}{v} \right]^2 = 0. \quad (6)$$

After mathematical manipulation, we have

$$\omega = \frac{v}{2} \sqrt{k_x^2 + k_z^2}, \quad (7)$$

and

$$d\omega = \frac{v}{2} \cdot \frac{k_z}{\sqrt{k_x^2 + k_z^2}} dk_z. \quad (8)$$

Plugging the above two equations into the equation of the inverse Fourier transforms at $t = 0$, we finally obtain the migrated data

$$s(x, z, t = 0) = \frac{1}{4\pi^2} \iint \frac{v}{2} \cdot \frac{k_z}{\sqrt{k_x^2 + k_z^2}} \cdot S(k_x, z = 0, \frac{v}{2} \sqrt{k_x^2 + k_z^2}) e^{jk_x x} e^{jk_z z} dk_x dk_z. \quad (9)$$

One thing to be kept in mind is the systematic errors in the migration techniques, which will lead to poor image reconstruction and inaccurate target position estimation even if the exact velocity distribution is used [13]. For example, the inherent assumption of circular wavefront neglects wave refraction at the interface and possible anisotropic antennas. Finding the exact wavefront itself is uneasy. The theoretical solutions to Maxwells equation for half-space problems are often too cumbersome to be applied. Even the resulting equations to find the refraction point at the interface for the simple-minded ray tracing method are of fourth-order. Recent attempts include correction on a point-to-point basis [46] and approximating the shape by hyperbola with parameters depending on medium dielectric constant, antenna height, and the propagation time from the source to wavefront [61]. The exact modeling of the problem is quite difficult, if possible. Another approach is to use experimental calibration to improve the results, which could be the future work. However, if the deviations from the true parameters are within the tolerance of the application, the results without calibration can still be acceptable for current usage.

2.1.2 Autofocusing Metrics

Automation is widely studied in various fields such as imaging and robotics [73][75] and autofocusing is a subcategory. Autofocusing techniques have been widely used in other fields such as optical imaging and SAR imaging. However, the adaptation of the autofocusing techniques to the GPR field has been much less investigated [32]. The very limited work for autofocusing techniques applied in common-offset GPR data are summarized here. The metric sharpness is applied for soil dielectric constant analysis [65] and later minimum support was proposed for the same application to conquer the inaccuracy caused by the uncertainty of the medium conductivity [66]. These techniques are only tested on simulated GPR data and both of them are technically semi-automatic because the process still involves human decisions for search areas and thresholds. Mean amplitude energy is adopted in [32] and it is proved to have less satisfying performance for GPR data from RC bridge decks. Remotely relevant work includes [83], which applied the minimum entropy method to localize subsurface objects and aimed to solve the problem of rough surface. In their work, the problem of slightly uneven homogeneous medium is transformed into a problem of lateral velocity variant medium. However, the prior information of nominal velocity is required and the model formalization is not theoretically rigorous.

In order to search suitable candidates for our application, autofocusing techniques from various fields are briefly reviewed first. The maximization of image sharpness was originally developed to correct phase errors in incoherent optical imagery [53]. Afterwards, a large volume of literature has targeted on the autofocusing techniques in SAR [12][28]. For GPR data migration, if the correct velocity distribution is used, the energy will be condensed into a few pixels for a point-like target; otherwise, it will spread into more pixels. This shares certain similarity with SAR autofocusing problems. After a broad review and careful study of the autofocusing techniques

available, the potential candidates for our application are summarized into the following groups: sharpness [50], support [66], intensity [50], entropy [45][74], contrast [12][48], and higher-order statistics [4]. The metrics based on sharpness and minimum support will not be further discussed as they are technically semi-automatic and still involve human decision of the segmented geometrical region around the targeted object and the threshold value. In addition, as there may be a cross rebar signals with high intensity and wide spread corrupting the cooperative targets, theoretically, these two techniques are not as appealing as other techniques although they can still work to some extent. The rest are introduced as follows [80]:

1. Averaged intensity techniques (AIT)

$$M3(k) = \frac{\sum_{i=1}^m \sum_{j=1}^n |s(x_i, z_j)|^k}{\left[\sum_{i=1}^m \sum_{j=1}^n |s(x_i, z_j)| \right]^k}, \quad (10)$$

where the index, k , can be 2 or 4, m and n represent the trace number and the number of sampled points per trace. When the index is 4, it is equivalent to the classic Muller-Buffington squared-intensity image sharpness metric [50]. A similar idea with a weight on each patch is later proposed in [28].

2. Entropy-based technique (EBT);

$$M4(k) = \sum_{i=1}^m \sum_{j=1}^n f(x_i, z_j) \ln [f(x_i, z_j)], \quad (11)$$

where

$$f(x_i, z_j) = \frac{|s(x_i, z_j)|^2}{\sum_{i=1}^m \sum_{j=1}^n |s(x_i, z_j)|}. \quad (12)$$

3. Image contrast-based techniques (ICBT)

$$M5(k) = \frac{\sqrt{\sum_{i=1}^m \sum_{j=1}^n \left\{ |s(x_i, z_j)|^k - \frac{1}{mn} \sum_{i=1}^m \sum_{j=1}^n |s(x_i, z_j)|^k \right\}^2}}{\sum_{i=1}^m \sum_{j=1}^n |s(x_i, z_j)|^k}, \quad (13)$$

where $k=1$ or 2 .

4. Higher-order techniques (HOT)

$$M6(k) = \frac{\sum_{i=1}^m \sum_{j=1}^n [|s(x_i, y_j)| - \hat{\mu}]^k}{(mn - 1)\hat{\sigma}^k} \quad (14)$$

where $k \geq 1$, $\hat{\mu}$ and $\hat{\sigma}$ are the mean and variance of the data.

2.2 Simulation Study

Before conducting experimental tests, simulation models are developed to study the performance of the metrics. The purpose is to systematically evaluate how the metric performance will react to possible deteriorating factors: noises, cross rebar interference, aperture width, or the mixed forms.

2.2.1 Simulation Setup

A segment of RC bridge deck is built in a GPR simulator, GprMax 2.0 [31], which is based on finite difference time domain (FDTD) method, and has been utilized by numerous researchers in the literature [64]. The RDP of the concrete is set to be 6.4 and the conductivity to 0.05 S/m. First a 2D model is simulated and the cross section is shown in Figure 1. The size of the concrete bridge deck is 2.436 m (8 ft.) wide and 0.216 m (8.5 in.) deep with an infinite length. A #5 rebar is buried at a depth of 6.35 cm (2.5 in.). The transceivers are two line source antennas with a common offset of 3 cm (bistatic acquisition mode) and a stand offset of 0.25 cm. The exciting source for the antenna follows a Ricker function with a center frequency of

2.6 GHz. Real GPR data from bridge decks are sometimes corrupted by cross rebar signals from the same rebar mat, which can be very strong and degrade the metric performance. The time range for each A-scan is 6 ns. The error of the simulation can be kept to a minimum if the discretization step is at least ten times smaller than the smallest wavelength of the propagating electromagnetic fields. To study the effects of cross rebar interference, a 3D simulation is also implemented. The reason the other simulation is not performed as a 3D model is that a 3D simulation will consume a much longer time, but generate basically visually the same radargrams as the 2D simulation. The 3D simulation setup is the same as the 2D model described above except a few minor differences explained as follows. First, another #5 rebar is placed directly on top of the rebar at 6.35 cm (2.5 in.), but oriented perpendicularly to it. Second, the scan line is parallel to the cross rebar and 2 cm away from the line right above the cross rebar. Third, the antenna is a Hertzian dipole, which is generally considered equivalent to a line source in a 2D model. As the radargrams from both 2D and 3D simulations are basically the same except that an extra bright band similar to the direct waves is overlapped with the hyperbolic curve in the image, only the generated raw profile from the 2D simulation collected with a step of 5 mm is shown in Figure 2.

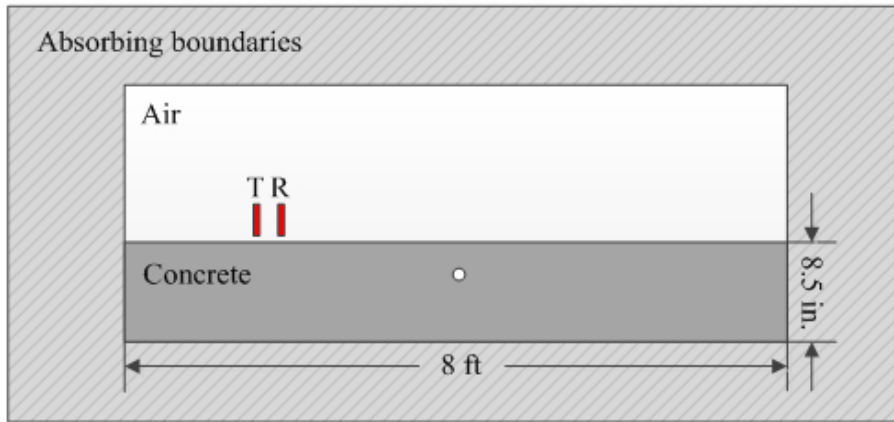


Figure 1: The cross section of the simulated RC bridge deck.

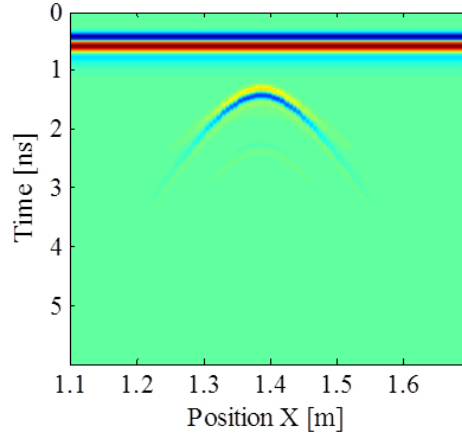


Figure 2: The original 2D GPR profile.

2.2.2 Preprocessing

A typical GPR dataset is composed of crosstalk, ground bounce, clutter, and rebar reflections. Crosstalk together with ground bounce (also called direct waves) usually exhibit high-intensity energy in the radargram, which can severely deteriorate the interpretation of the reflected signals from buried targets and they are usually removed by the preprocessing. The two most popular methods for that are time gating and background average removal. The former is more suited to uneven surfaces, but will lose target information if the target is too shallow and the target signals are mixed with the direct waves; the latter has less harm to shallow target signals, but tends to degrade rapidly for moderate roughness. Interference removal techniques are under pursue for unfavorable situations and will be discussed in Chapter III. In this section, the simulation data is preprocessed by time gating as the direct waves are not mixed with the target signals while the average removal will leave an artificial line for the pixels along rows exhibiting relatively strong target signals. For the experimental data, background average removal is applied instead as the direct waves are mixed with the target signals. In addition to the removal of direct waves, usually the time-zero also needs to be determined. Multiple determination approaches for the time-zero are summarized in the [60]. A simple commonly adopted approach is

to take the instant value where the Ricker wavelet attains the maximum of the first peak. However, this factor will not be taken into account as it can be calibrated together with other factors such as the antenna distance, stand offset, and systematic errors in the migration process mentioned above, as it does not observably affect the image quality. In addition, the simulation results show that the obtained RDP value is already very close to the true value. The preprocessed radargram from the simulation is shown in Figure 3, where the strong direct waves are efficiently removed.

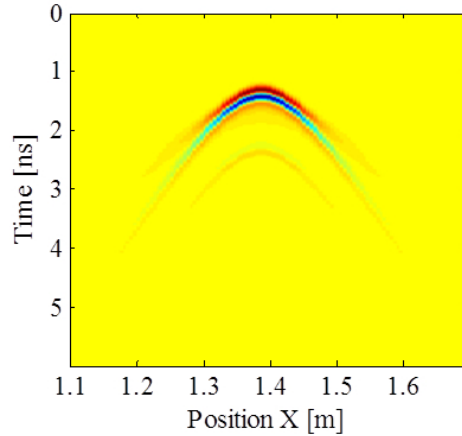


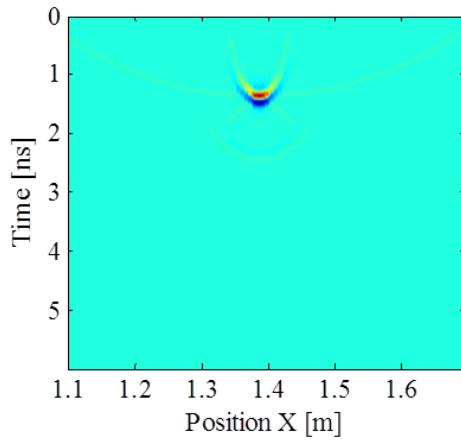
Figure 3: The preprocessed GPR profile.

2.2.3 Results and Discussions

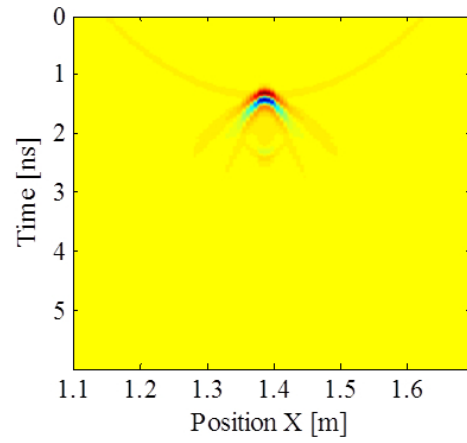
2.2.3.1 Clean Radargram

The migration results with different velocities are shown in Figure 4. We can see that the rebar signal is well focused in Figure 4(c) with the accurate velocity, and a migration smile and a frown are formed in Figure 4(a) and 4(b) when the migration velocity is set too high and too low, respectively. The variation of the above normalized metric values (NMV) with the changing RDP is shown in Figure 5. For the HOT, the index is selected to be 10 for illustration. Figure 5 shows all metrics give a maximum value around the medium RDP. Reasonable error toleration should be given as the results are not calibrated yet. The sensitivity varies among different metrics: M6(10) gives the highest sensitivity and then followed by M3(4), M4(1),

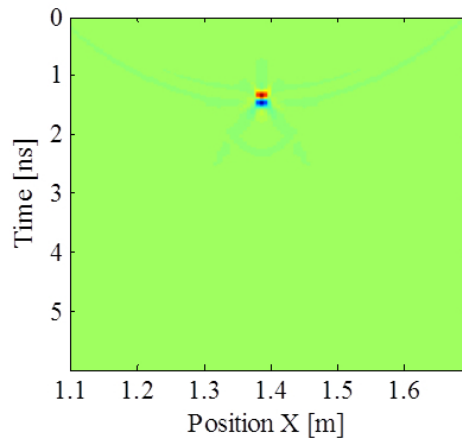
M5(2), M3(2), and M5(1).



(a)



(b)



(c)

Figure 4: Migrated profiles with (a) a higher velocity, (b) a lower velocity, and (c) the real velocity.

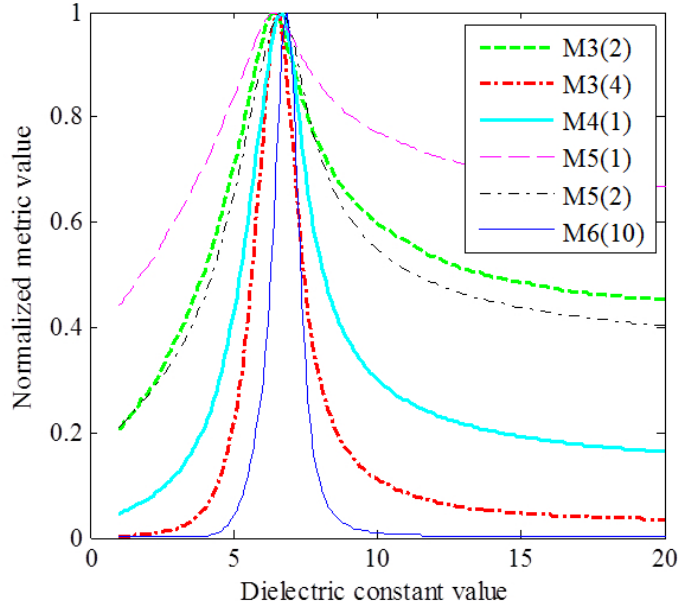


Figure 5: Metric performance for the clean GPR profile.

2.2.3.2 Noise

Different levels of Gaussian noise is added using the Matlab function `awgn`. A Monte Carlo simulation is performed for noise related tests and consistent results are demonstrated here. A polluted radargram is shown in Figure 6, where it is a bit difficult to perform visual inspections. The performances of autofocusing metrics for SNR=-30dB, -55dB, and -60dB are shown in Figure 7. The results show that for a higher SNR (SNR=-30dB), all metrics reach a maximum value around the true value of the medium RDP. With the increasing of noise, M6(10) is much less affected whereas other metrics deteriorate faster. M3(2) and M5(1) first lost the track of the optimal value when the SNR hits -55dB. When the SNR reaches -60dB, all the metrics fail. The ability to stand lower SNR makes M6(10) a more robust autofocusing metric. The sensitivity order of the metrics generally does not change with different SNR levels. As the real noise distribution of the concrete may be difficult to model, other available noise types are also investigated and the rank of the metrics is quite similar. An example of the GPR profile with salt and pepper noise is shown in Figure 8 and

the corresponding metric performance is shown in Figure 9.

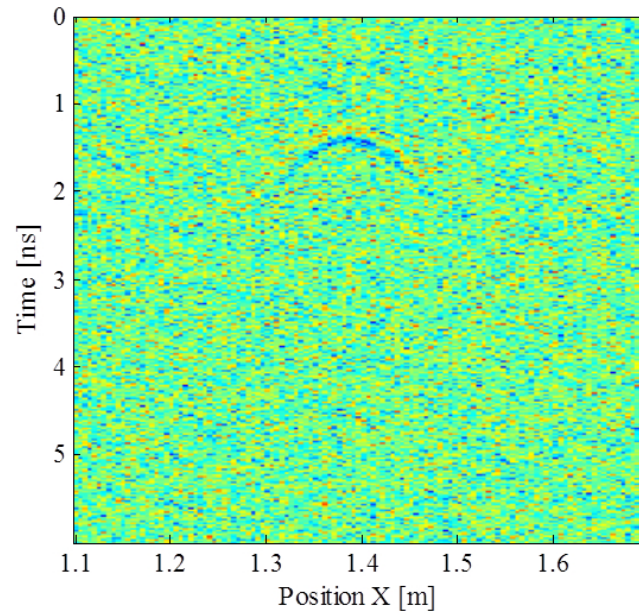
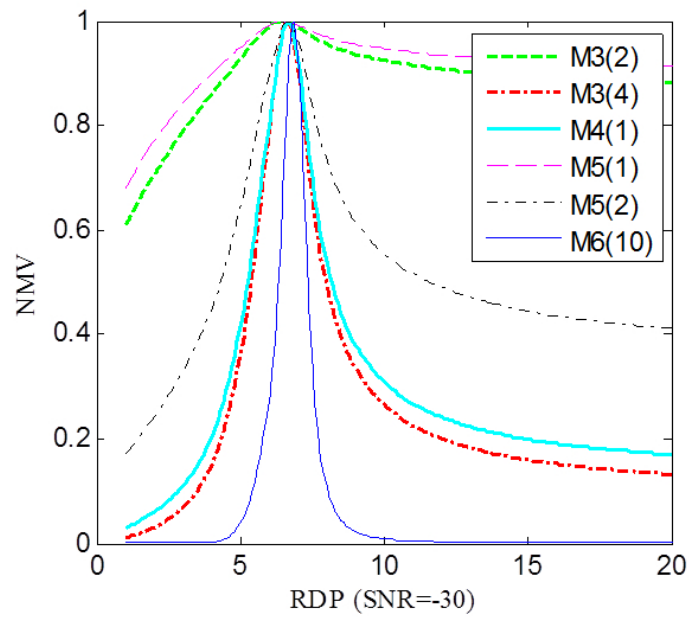
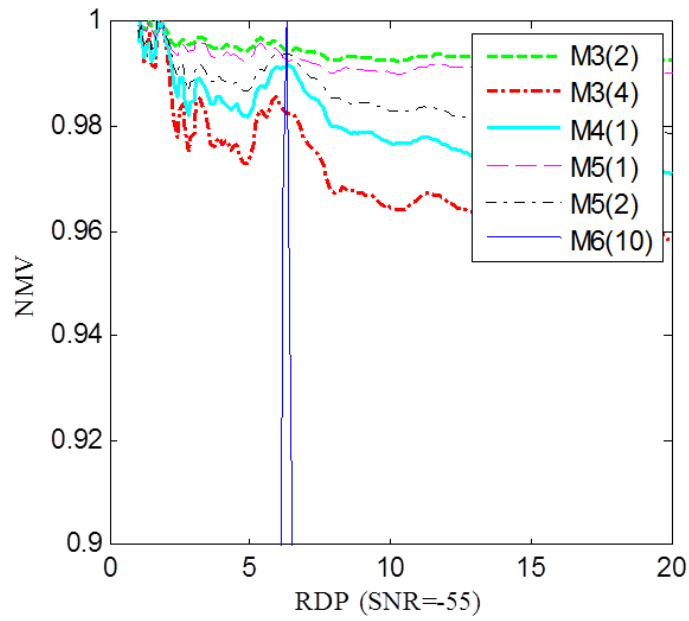


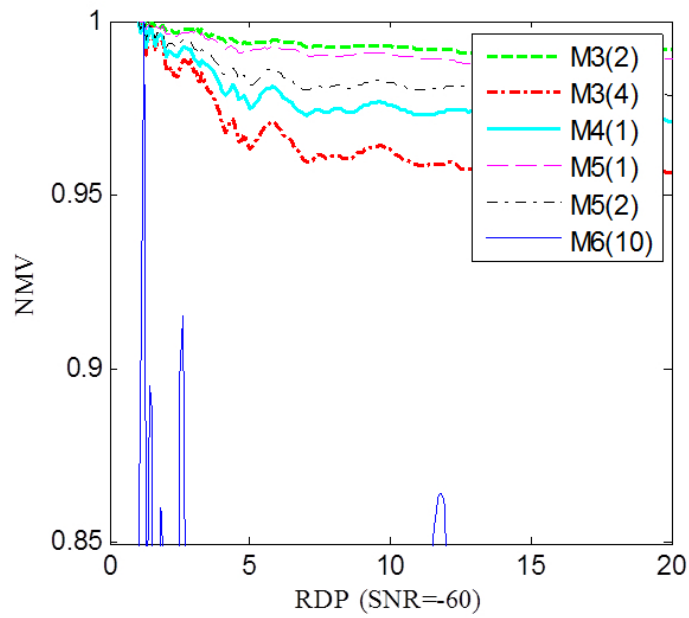
Figure 6: GPR profile with white noise (SNR=-50).



(a)



(b)



(c)

Figure 7: Metric performance for (a) SNR=-30dB, (b) SNR=-55dB, and (c) SNR=-60dB.

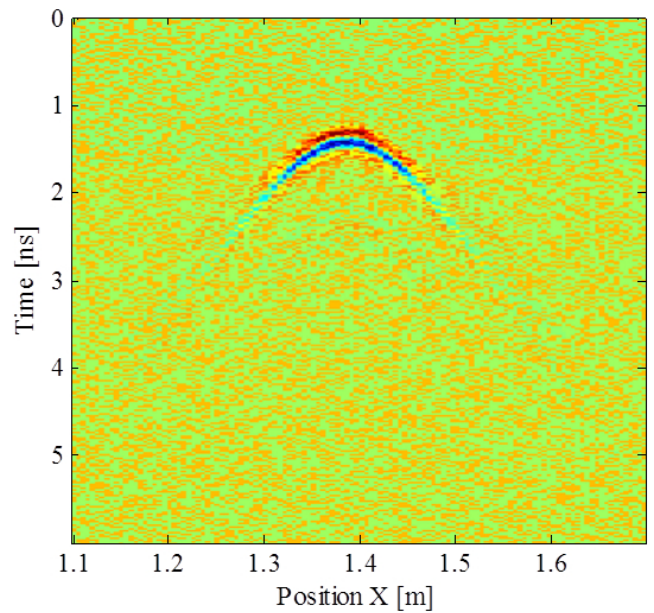


Figure 8: GPR profile polluted with salt and pepper noise.

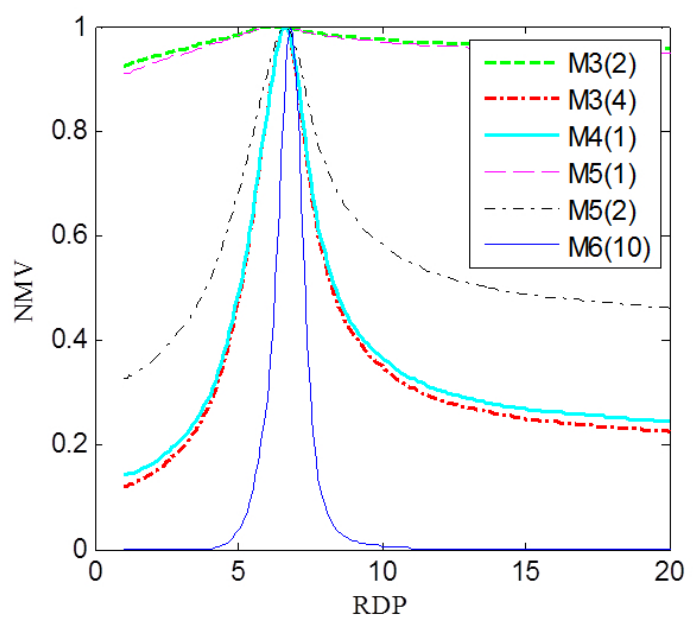


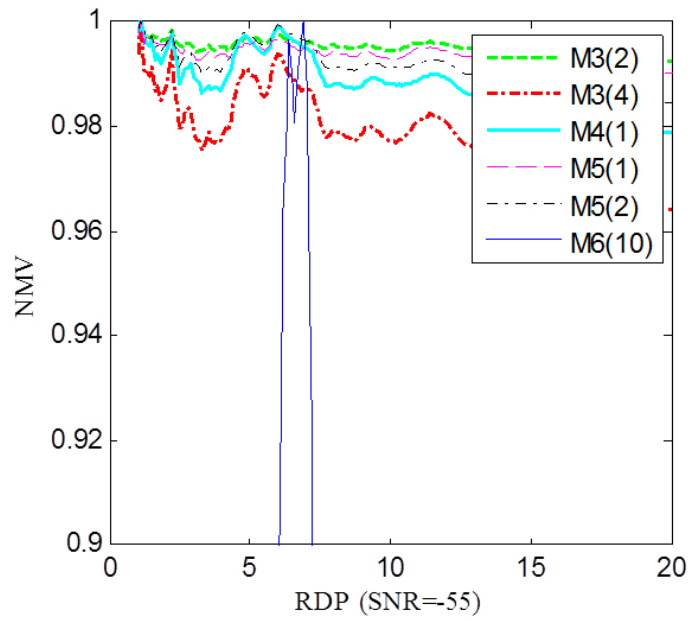
Figure 9: Metric performance for GPR profile with salt and pepper noise.

2.2.3.3 Aperture Width

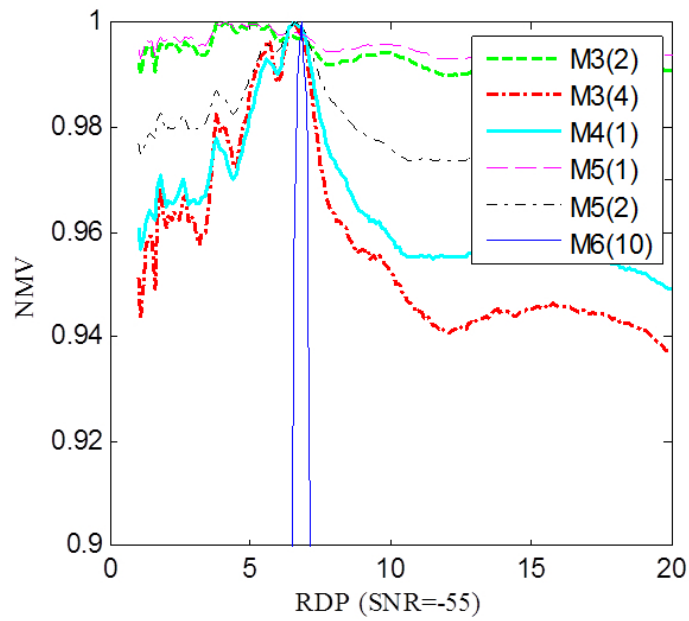
The hyperbolic curve has two long decreasing arms. How to confine the search field needs to be taken into consideration. For clean data, the performance should be better with larger apertures. Results show that the sensitivity of all metrics may decrease with smaller aperture and even fails for very small aperture or heavily biased apertures. However, for noisy data, more noise will be included with larger apertures. An example is shown in Figure 10 for SNR=-55dB, where a smaller aperture actually provides a better performance for the same dataset. For our experimental data, the radargram is segmented according to the rebar intervals and results demonstrate that the aperture width is adequate for current usage.

2.2.3.4 Cross Rebar + Noise

The real GPR data from bridge decks are sometimes corrupted by cross rebar signals from the same rebar mat, which can be very strong and degrade the metric performance. By comparing Figure 7 and Figure 11, we observe that the interference of the cross rebar degrades the sensitivity of the metrics and they lose the effectiveness faster with increasing noise than the cases without cross rebar signals. Compared to other metrics, M6(10) is much less affected. The conclusion is that the interference of the cross rebar signals deteriorate the metric performance in both aspects of sensitivity and robustness.

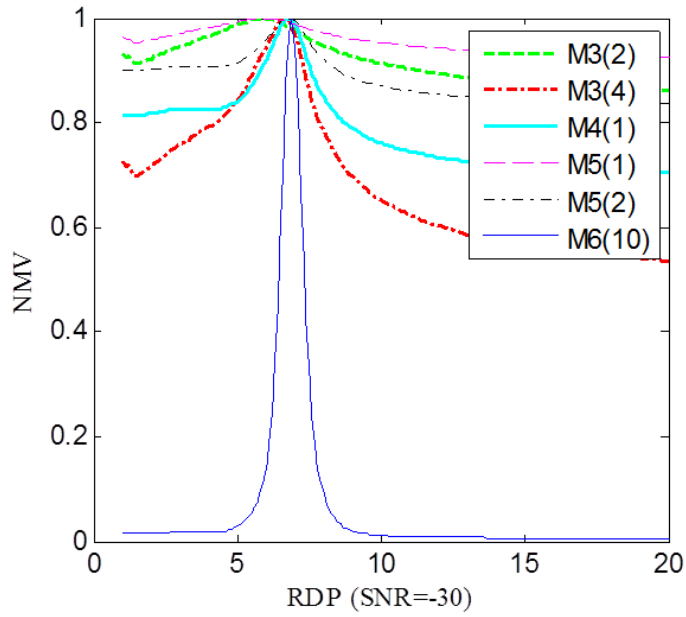


(a)

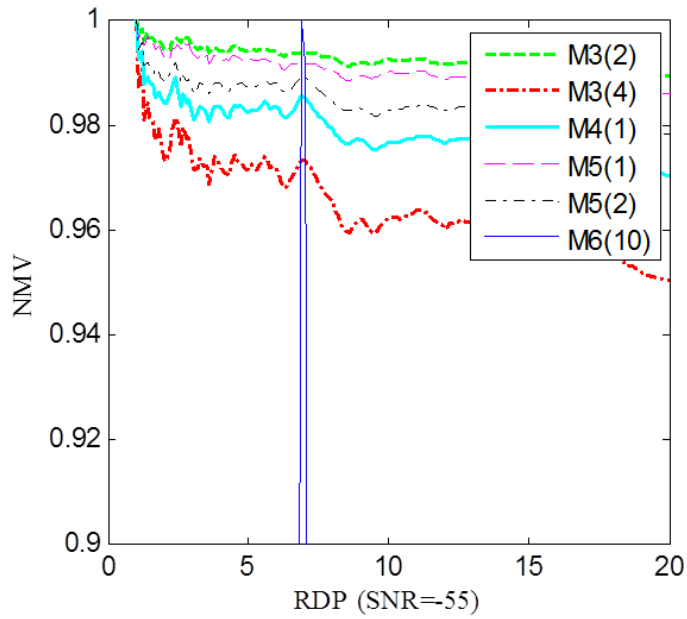


(b)

Figure 10: Metric performance for data with the aperture width of (a) 100 traces and (b) 30 traces.



(a)



(b)

Figure 11: Metric performance for data with the cross rebar reflections and (a) SNR = -30dB and (b) SNR = -55dB.

2.3 Experimental Study

2.3.1 Experimental Setup

A bridge deck section was prepared at the University of Texas at El Paso, as part of a research project to compare NDT technologies for RC bridge decks [33]. A bird's-eye view of the deck is shown in Figure 12. The concrete deck has dimensions of 6.09 m (long) \times 2.436 m (wide) \times 0.216 m (deep) (20 ft. \times 8ft. \times 8.5 in.), which is large enough to simulate a full scale bridge deck. In addition, the deck is embedded with two mats of uncoated steel rebars at the depths of 6.35 cm (2.5 in.) and 15.24 cm (6 in.). The reinforcement mats are composed of #5 rebars spaced at 20.32 cm (8 in.) in the transverse direction and 25.4 cm (10 in.) in the longitudinal direction. A Texas Department of Transportation (TxDOT) class S concrete mixture was used for the deck construction. Artificial delaminations made of soft polyester fabric and foams are placed on the rebar mats. For more details of the deck, please refer to [43]. The GPR data were collected every 5 mm using the GSSI SIR-20 acquisition system equipped with 2.6 GHz antennas. Detailed information about GSSI GPR acquisition systems and antennas is available on the GSSI official website [2]. The time window is 12 ns and the number of sampled data per scan is 1024. The first dataset to be demonstrated are collected along the vertical line at 3.65 m (12.00 ft.) along the horizontal axis as it has strong reflections from a cross rebar. For comparison, the second dataset to be demonstrated are collected along the vertical line at 3.72 m (12.25 ft.) along the horizontal axis, which is away from cross rebars.

2.3.2 Results and Discussions

The raw and preprocessed GPR profiles for the first dataset are shown in Figure 13. Figure 14 gives an example of migrated results with a constant velocity. It can be observed that the leftmost rebar is appropriately migrated, but others are undermigrated at different levels, which indicates that our slab cannot be treated

as homogenous. First to segment the radargram with respect to each rebar, and then search the RDP separately using the autofocusing metrics and concatenate the appropriately migrated piecewise profiles is proposed. For illustration, the variations of NMV with changing RDP for the leftmost rebar are shown in Figure 15. All the results show that the higher-order metric, M6(10), gives the best results in terms of robustness and sensitivity. M3(2) and M5(1) fail for most experimental data. Other metrics give moderate results but the search field of the RDP might need to be narrowed if fully automated. The obtained RDP distribution with M6(10) as the autofocusing metric is shown in Figure 16(a) and the corresponding migrated profile is shown in Figure 16(b), where all the rebar signals are well focused. The y-axis is denoted by time and it can be readily translated into depth information with the obtained velocity distribution. It can be observed that the RDP value varies monotonically from one side of the bridge deck to the other side. One possible reason for this is presented here. The deck is water-cured during its fabrication process and the GPR data is collected shortly after its fabrication [43]. The deck may have not been positioned absolutely flat, and hence this will affect the moisture/water distribution. If the deck is tilted slightly to one side, it is possible to result in the phenomenon here as the RDP of water is quite high compared to dry concrete, and hence can easily affect the permittivity of the structure.

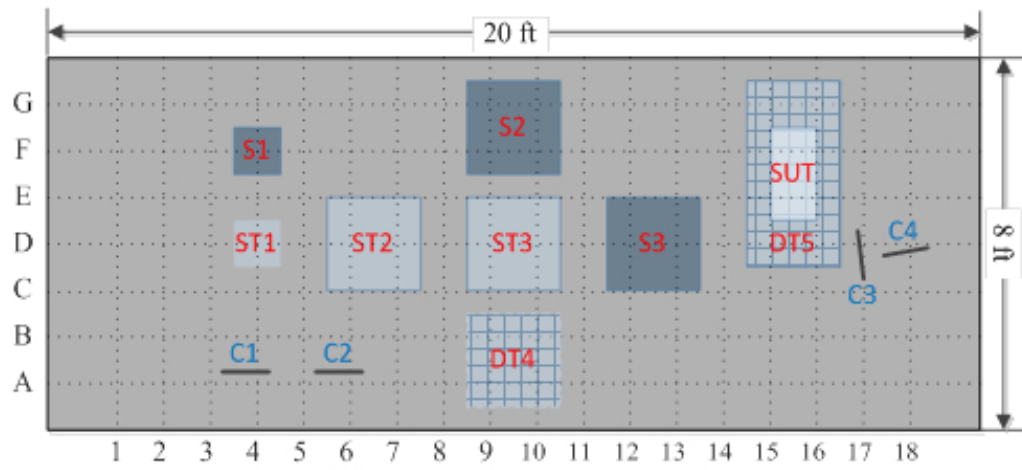
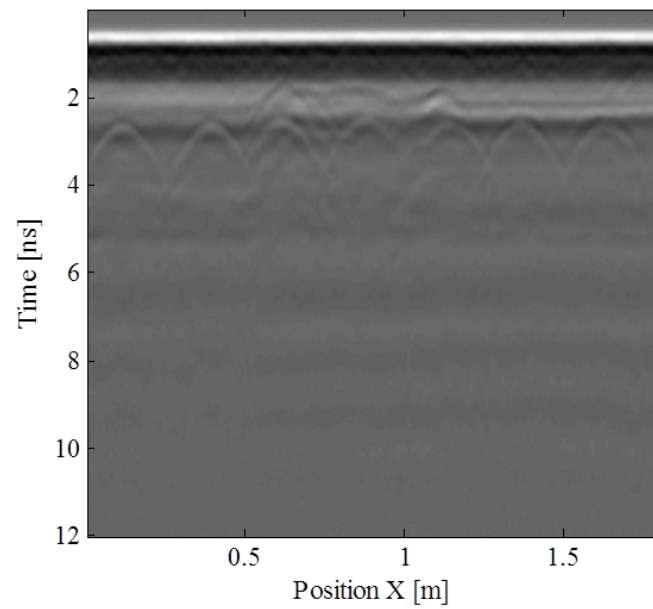
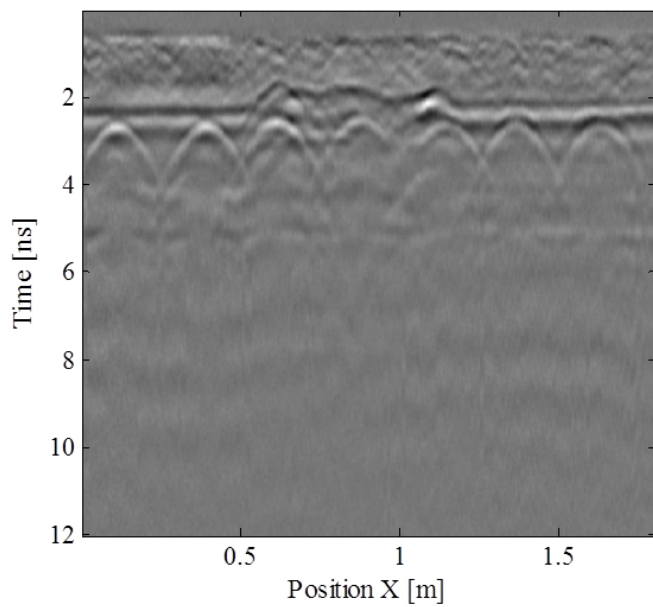


Figure 12: The bird's-eye view of the fabricated RC bridge deck.



(a)



(b)

Figure 13: (a) The original profile and (b) the preprocessed profile of the GPR data collected along the vertical line at 3.65 m (12.00 ft.) along the horizontal axis.

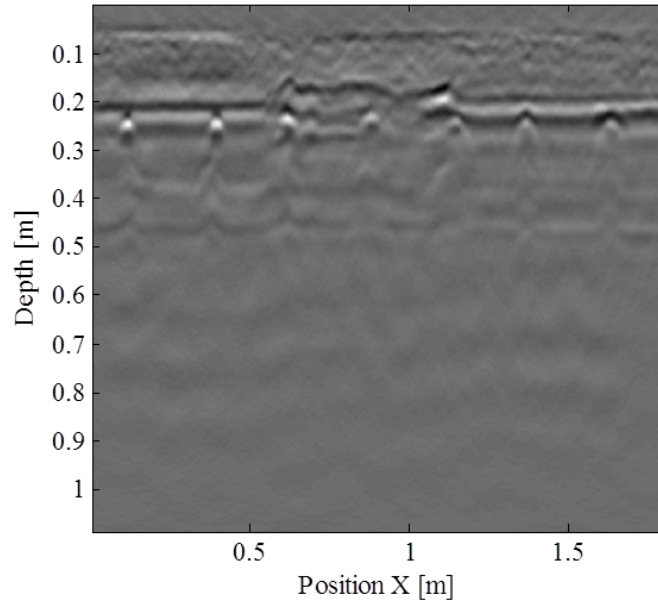


Figure 14: The migrated GPR profile with a constant velocity.

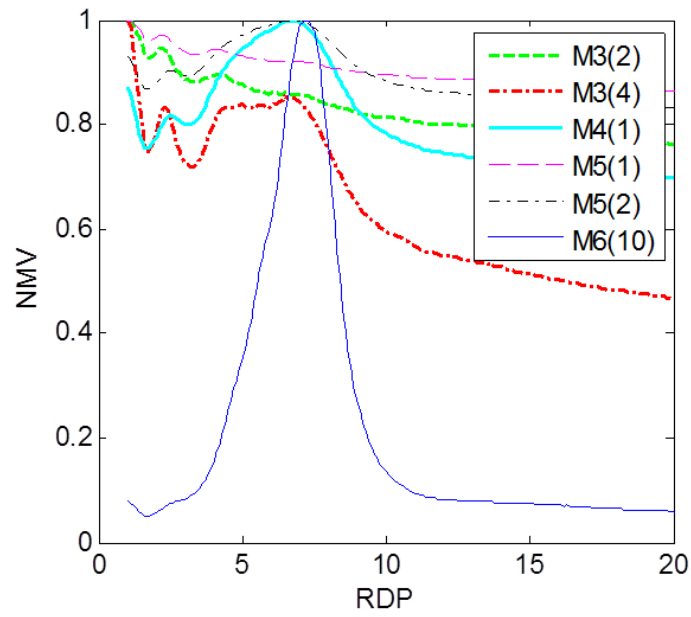
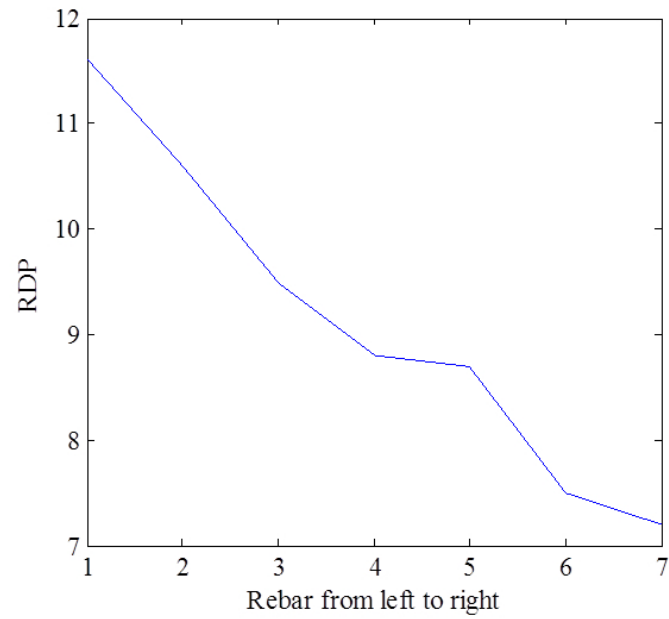
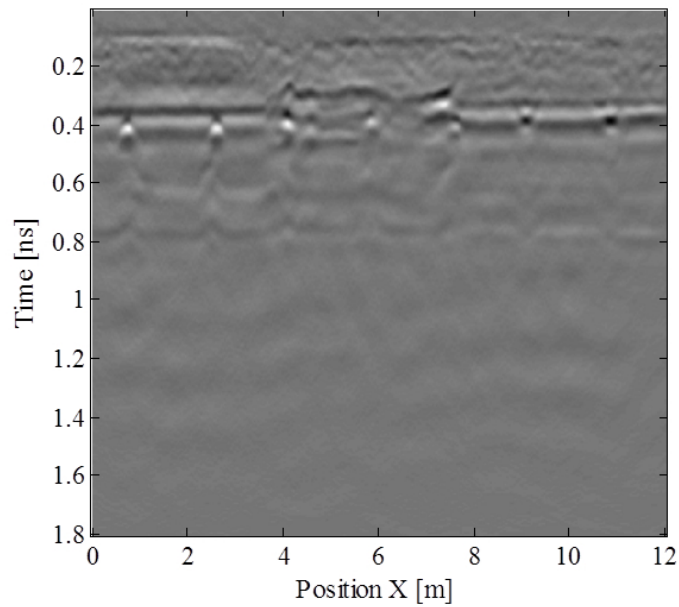


Figure 15: Metric performance for the leftmost rebar.



(a)

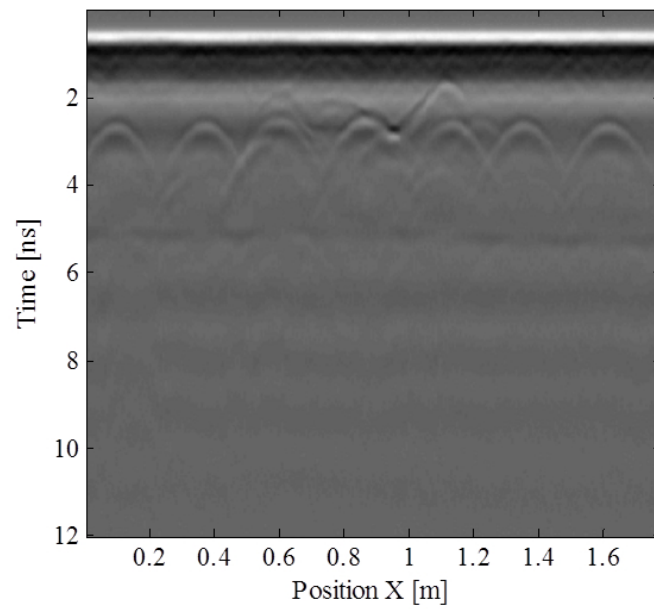


(b)

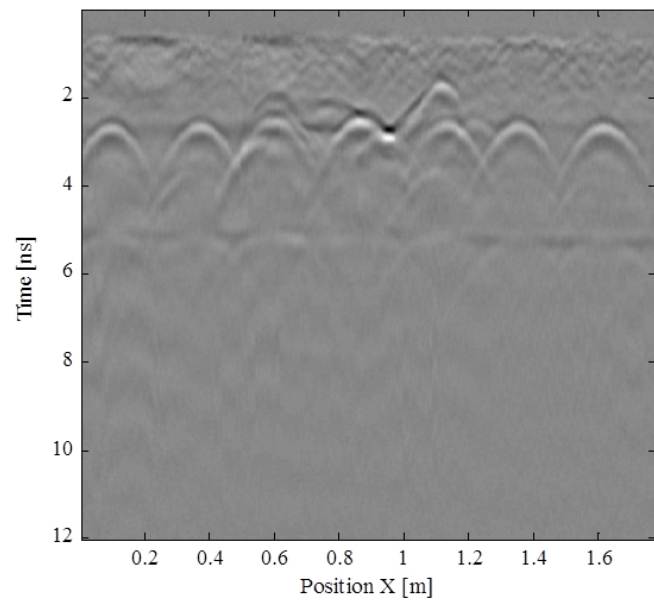
Figure 16: (a) The optimized RDP distribution and (b) the corresponding migrated GPR profile.

To illustrate the interfering effect of cross rebar signals, another GPR profile that is collected along a test line further away from cross rebars is also demonstrated here. The raw and preprocessed GPR profiles are shown in Figure 17(a) and 17(b), respectively. Comparing with the GPR profile in Figure 13, the GPR profile here is less affected by the nearby cross rebar signals. The variations of all autofocusing metrics with changing RDP values for the rightmost rebar are shown in Figure 18(a). The performance of all autofocusing metrics is better than that in Figure 15, which resulted from applying autofocusing metrics to the GPR profile with strong cross rebar interferences. As indicated in the simulation study, larger apertures may improve the performance of autofocusing metrics for clean data, but the metrics performance may get better if the aperture size is decreased for experimental data because of the ubiquitous existence of noise. It is suggested not to adopt an aperture size bigger than the rebar interval as it will bring in neighboring rebar signals. The metric performance with a smaller aperture size is shown in Figure 18(b). In this case, it does not provide noticeable improvement. Therefore, it is generally considered appropriate to adopt the rebar interval as the aperture size.

The experimental results are consistent with the simulation study although the experimental data come from a more complicated situation. The optimal dielectric constant values obtained from different metrics vary a little bit from each other, but they can still be considered within error tolerance for the purpose of imaging. The RDP distribution with higher precision can be obtained with accurate modeling or experimental calibration.

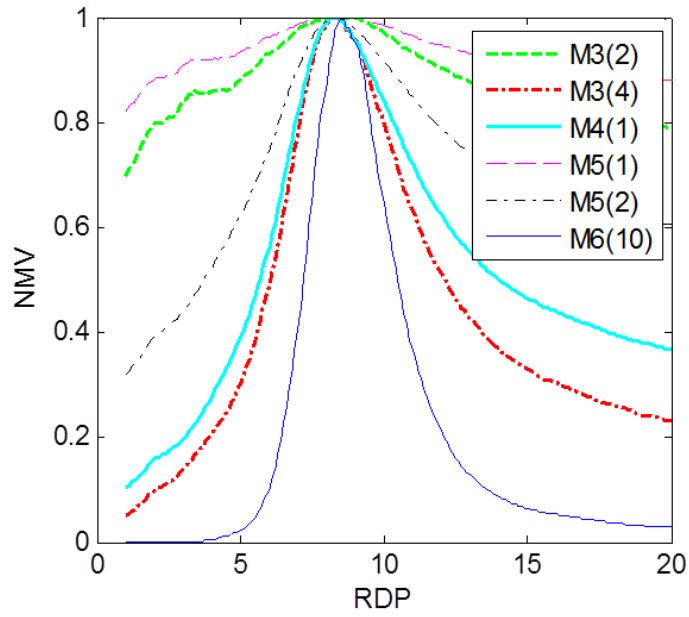


(a)

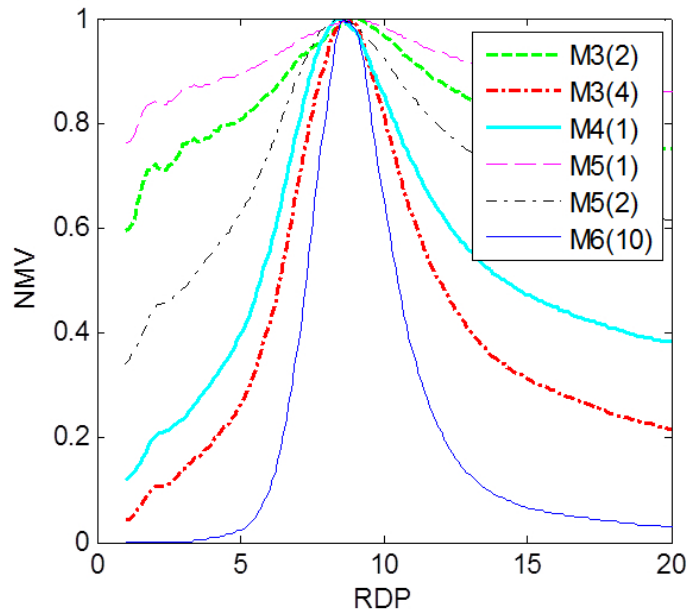


(b)

Figure 17: (a) The original profile and (b) the preprocessed profile of the GPR data collected along the vertical line at 3.72 m (12.25 ft.) along the horizontal axis.



(a)



(b)

Figure 18: Metric performance for the rightmost rebar (a) with the full aperture and (b) with 30 traces less.

2.4 Summary

In this section, multiple autofocusing metrics are introduced and evaluated for the automatic velocity analysis of bistatic GPR data from RC bridge decks. The metrics are first evaluated under various simulated conditions to study how potential factors associated with the RC bridge deck inspection (noise, aperture width, and cross rebar signal) affect the metric performance. The results show that the higher-order metrics are the most robust and sensitive metric among them, and can even generate satisfying results for severely polluted data where visual inspections cannot be performed. Similar conclusions can be drawn from the experimental study. In the experimental study, the RDP distribution with high resolution is obtained automatically, and all rebar signals are well focused in the correspondingly migrated profile. The determination of the RDP distribution is not only important for image quality, but also for the material property estimation, which is helpful for the bridge deck assessment.

CHAPTER III

INTERFERENCE REMOVAL

3.1 Proposed Approach

In this thesis, we proposed an approach based on F-K filtering to remove direct waves from uneven surface and cross rebar reflections from inhomogenous medium. F-K filters belong to the category of velocity filters, which have been widely used in the seismic field [19][69]. A velocity filter, applied in the F-K domain, is also known as apparent velocity filter, fan filter, dip filter, slope filter or Pie-Slice filter. The principle is based on the differences of apparent velocities, which equal to the slopes in the F-K fields, caused by different events. It is brought up in seismic field by [25] to separate events with different dipping angles in structurally complex areas and suppress certain types of unwanted energy that obscure primary reflections such as high-velocity noise and wideband multiples in areas where a normal-moveout contrast exists between primaries and multiples. Coherent linear events, such as ground roll, guided waves, and side scattered energy, can also be separated in the F-K domain accordingly [56]. It has been recently introduced into the GPR field by [39]. In their paper, F-K filters are adopted to remove the crosstalk generated by a bistatic system. The bistatic system uses a horn antenna as a fixed transmitter and an optical electric field sensor as a receiver running over the testing field. With this setup, the arrival time for the direct waves is different from trace to trace. Two filters are designed in their paper. One is to calculate the apparent velocity range according to the exact information of the receiver and filter this fan area in the F-K domain; the other is to first align all the traces according to the arrival times of the cross talk, and then to reject the dc component in the spatial frequency direction, which represents the

signals with infinite apparent velocity and is equivalent to the frequency axis in the F-K domain. However, both designs of the filters require the prior information of the exact transmitter and receiver locations for the whole scanning process, and only work for cases where the surface is flat and the medium is homogeneous. Similar ideas are then followed up by [88][18].

Inspired by [39], we come up with an idea to remove cross talk together with ground bounce from rough surface by taking into account the small dipping angles and call this process dip relaxation [81]. The reason we can bring this process into F-K filtering is that our target signals are scattered over a wide span along the spatial frequency direction in the F-K domain, which means they exist in areas representing a wide range of apparent velocity values (large dipping angle range) while the rough surface composed of small plane reflectors with a much narrower dipping angle range. In addition, the cross rebar signals can also be modeled as slightly distorted uneven reflectors with small dipping angles considering the variations of wave propagation velocity through the heterogeneous medium, concrete, is not dramatic. The mechanism of the previous design of the F-K filter and the correctness of the target modeling are illustrated using a simple GPR simulation dataset. The effectiveness of the F-K filter with adequate dip relaxation is validated by both experimental and field GPR data. In addition, the performance of the proposed method is compared with that of the background subtraction (BS) method. Although both the BS and the subspace projection methods are considered as gold standard approaches and a new clutter removal method should be compared with them, they have been demonstrated to have similar performance in [67]. Our proposed method will be compared with average removal in this thesis.

3.1.1 Theory of F-K Filtering

The principle of F-K dip filtering, to put it in a simple way, is based on the fact that the apparent velocity equals the slope through the origin in the F-K domain. The apparent velocity along the x-axis can be defined as:

$$v_{ap} = \frac{v}{\sin \theta} \quad (15)$$

where v is the wave propagation velocity; θ is the dipping angle, namely, the angle between the horizon and the reflector. In an ideal case assuming the bridge deck surface is smooth and exactly flat, the dipping angle will be zero, and the apparent velocity of the direct wave, equivalent to the slope in the F-K domain, will be infinity. In our application, the target signals are the rebar reflections. Normally, the GPR survey path is perpendicular to the orientation of the targeted rebar. Since the cross section of a rebar can be approximately treated as round shaped, imagining the multiple tangent lines around the circle, the reflections from tangent points on the circle corresponds to reflectors with the dipping angles vary continuously from zero to 90 degree. This is equivalent to areas confined by slopes of reflected rebar signals in the F-K domain vary from infinity to v . Because the energy of the direct waves is concentrated on the frequency axis while the energy of the target is scattered over a wide span along the spatial frequency direction in the F-K domain, the direct wave can be eliminated by removing the energy along the frequency axis and the loss of target signals is negligible from this operation.

The process of the F-K filtering is generally composed of four steps. First, let $s(x, z = 0, t)$ be the collected two-dimensional (2D) radar record, and it is transformed to its representation in the F-K domain by applying 2D Fourier transform:

$$S(k_x, z = 0, \omega) = \iint s(x, z = 0, t) e^{-jk_x x} e^{-j\omega t} dx dt. \quad (16)$$

Second, design the reject zone in the F-K domain and mute both the amplitude and phase spectrum to zero in this region. For the ideal case, the expression for the filter

in the F-K domain is

$$H(k_x, \omega) = \begin{cases} 0 & \text{if } k_x = 0 \\ 1 & \text{otherwise} \end{cases} \quad (17)$$

Third, apply the designed F-K filter to the input dataset by multiplication:

$$G(k_x, z = 0, \omega) = S(k_x, z = 0, \omega) \cdot H(k_x, \omega), \quad (18)$$

where $G(k_x, z = 0, \omega)$ is the filtered GPR record. Last, the time-spatial (T-X) radar profile after interference removal, $s_f(x, t)$, is recovered by applying 2D inverse Fourier transform to $G(k_x, z = 0, \omega)$:

$$s_f(x, t) = \frac{1}{4\pi^2} \iint G(k_x, z = 0, \omega) e^{jk_x x} e^{j\omega z} dk_x d\omega. \quad (19)$$

Spatial aliasing is a practical issue associated with 2D Fourier transform for both Stolt migration and F-K filtering [56]. The formula for determining the maximum frequency that can be handled without spatial aliasing is given by:

$$F_{max} = \frac{v}{2dx \sin(\theta)} \quad (20)$$

where dx is the trace spacing. F_{max} reaches its smallest possible value when the numerator reaches the smallest value and the denominator reaches the largest value. The largest value for $\sin \theta$ is 1. The trace spacing for GPR testing of bridge decks is usually around the magnitude of centimeter or millimeter [33][59]. For the experimental data shown in this thesis, the trace spacing is 0.005 m and the relative dielectric constant is less than 13, which lead to a velocity of 8.3e7 m/s. This leads to a value of 8.3 GHz for the lower limit of the maximum unaliased frequency. The antenna center frequency used in the experiment is 2.6 GHz, which indicates that the maximum frequency needs to be considered is 7.8 GHz [31]. Therefore, we do not need to worry about spatial aliasing for this application. The same holds for the field data.

3.1.2 Dip Relaxation

In real cases, the ground or the bridge deck surface is not smooth and flat. In this paper, we model this situation by introducing moderate dip relaxation in the F-K dip filter. The filter, $H(k_x, \omega)$, is modified as:

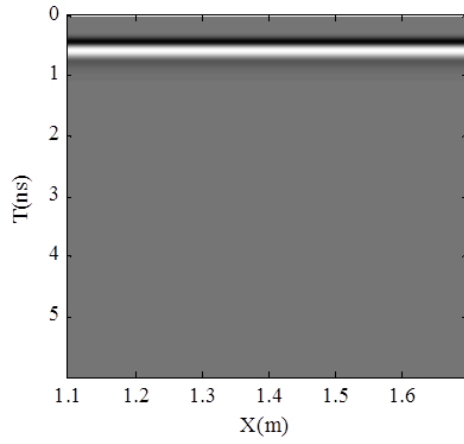
$$H(k_x, \omega) = \begin{cases} 0 & \text{if } (\omega/k_{xr} \leq \omega/k_x \leq +\infty) \\ 1 & \text{otherwise} \end{cases} \quad (21)$$

where ω/k_{xr} is the slope determined by the maximum dip angle relaxation. For example, if the dip relaxation is 30 degree, ω/k_{xr} is $2v$. Moreover, as indicated by our previous paper, cross rebar signals are another hinder for the performance of the autofocusing techniques. Theoretically, the dipping angle of the cross rebar is zero and its signal should correspond to the energy on the line with the slope of infinity through the origin in the F-K domain, similar to the case of ideal direct waves. In real RC bridge deck applications, the medium through which the wave propagates sometimes cannot be considered as homogenous. The crossing rebar signals from inhomogeneous medium or rough surface exhibit as a distorted uneven line in the GPR profile, as can be shown later by both the experimental data and the field data. One of the reason is the different TWTs caused by the variations of the medium permittivity along the scanning line. In this paper, we transform the problem of even reflectors in the inhomogeneous medium under rough surface into the problem of rough reflectors. Assuming there is no abrupt change in the medium property, which is a reasonable assumption in real cases, the dip angle relaxation can also be confined to a small angle and the target signals will not be affected much by the dip filtering.

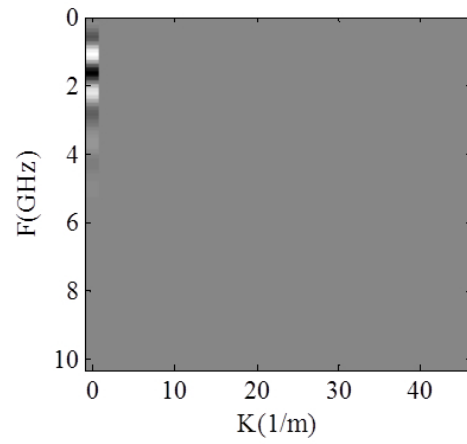
3.2 Simulation Demonstration

The simulation setup is the same 2D model as previously described. First we transform the data with only direct waves (Figure 19(a)) and only target signals (Figure

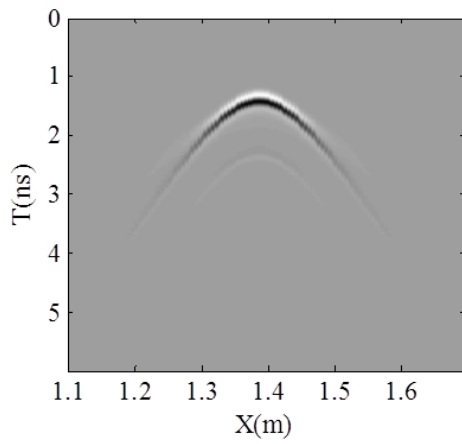
19(c)) into their respective F-K domains (Figure 19(b)) and 19(d)). It can be observed that the direct waves in the F-K domain are concentrated in the left corner while the target signals are spread over a wide range along the spatial frequency direction. This is consistent with the theoretical analysis above. Based on this information, we only need to apply the simple F-K filter to remove the direct waves along the frequency axis. Although the first column also has a small amount of the target signal, the loss is negligible. The resulted GPR profile after F-K filtering is shown in Figure 20(a). As a comparison, the commonly used background subtraction (BS) method is also used to remove the direct waves and the result is shown in Figure 20(b). As expected, the GPR profile after F-K filtering generates basically the exact signals as we wanted while the profile after BS method creates artifacts.



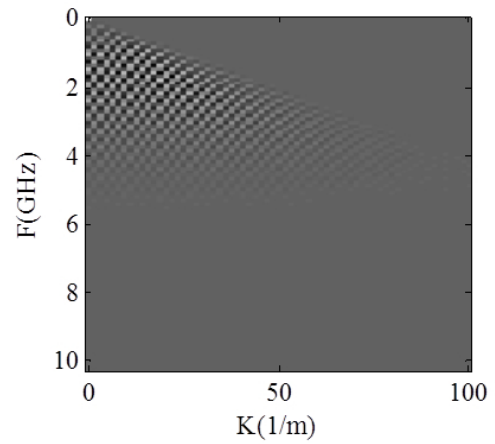
(a)



(b)



(c)



(d)

Figure 19: Simulated GPR profiles with (a) only direct waves in the T-X domain and (b) in the F-K domain; (c) only target signals in the T-X domain and (d) in the F-K domain

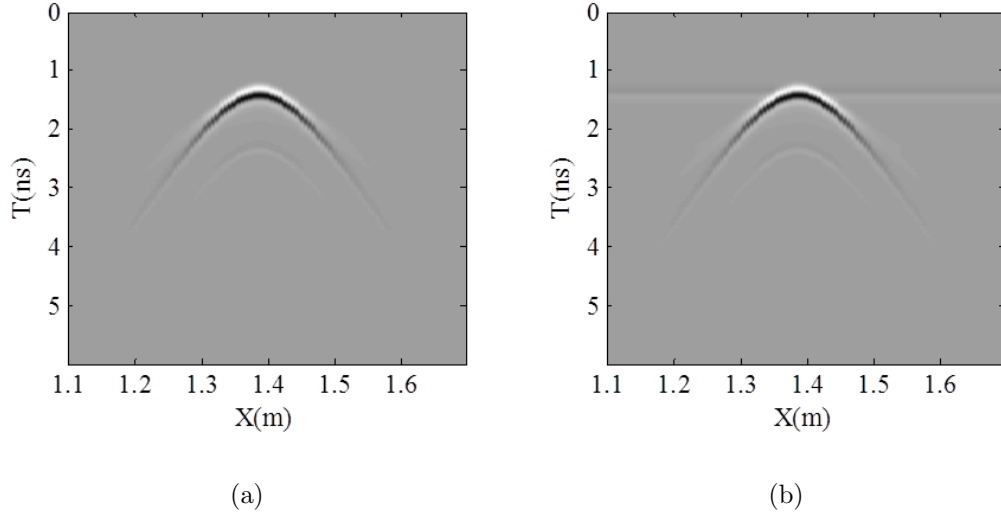


Figure 20: Simulated GPR profiles after (a) F-K filtering and (a) BS.

3.3 *Experimental and Field Study*

3.3.1 Data Collection

The experimental data is collected on a segment of concrete bridge deck fabricated in the lab environment. The demonstrated data is collected along the vertical line at 3.65 m (12.00 ft.) along the horizontal axis on the same fabricated slab as described in the previous chapter and the raw data is shown in Figure 21. The field data is collected on a real bridge deck in service, the Route 15 bridge over I-66 in Haymarket, Virginia. Bridge selection and organization of testing were done in collaboration with the FHWA’s Long-Term Bridge Performance (LTBP) Program, Virginia Department of Transportation, and Virginia Transportation Research Council. The Haymarket Bridge is a two-span concrete deck on a steel girder structure and was constructed in 1979. The bridge has a 15 degree skew. The reinforced concrete deck is about 8 in. thick. Testing was conducted on a 25.54 m (84 ft.) by 3.65 (12 ft.) area, marked in red in Figure 22, extending over parts of the shoulder and travel lane. GSSI’s GPR data collection system with 1.5 GHz ground-coupled antenna is used for data collection. For more detailed information about the field test, please refer to [33].

The raw profile for demonstration is shown in Figure 23.

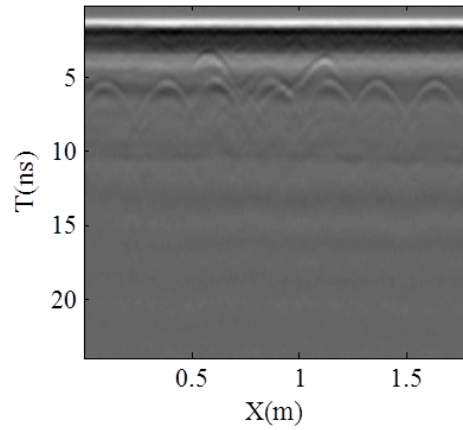


Figure 21: The original GPR profile collected from the experimental specimen.

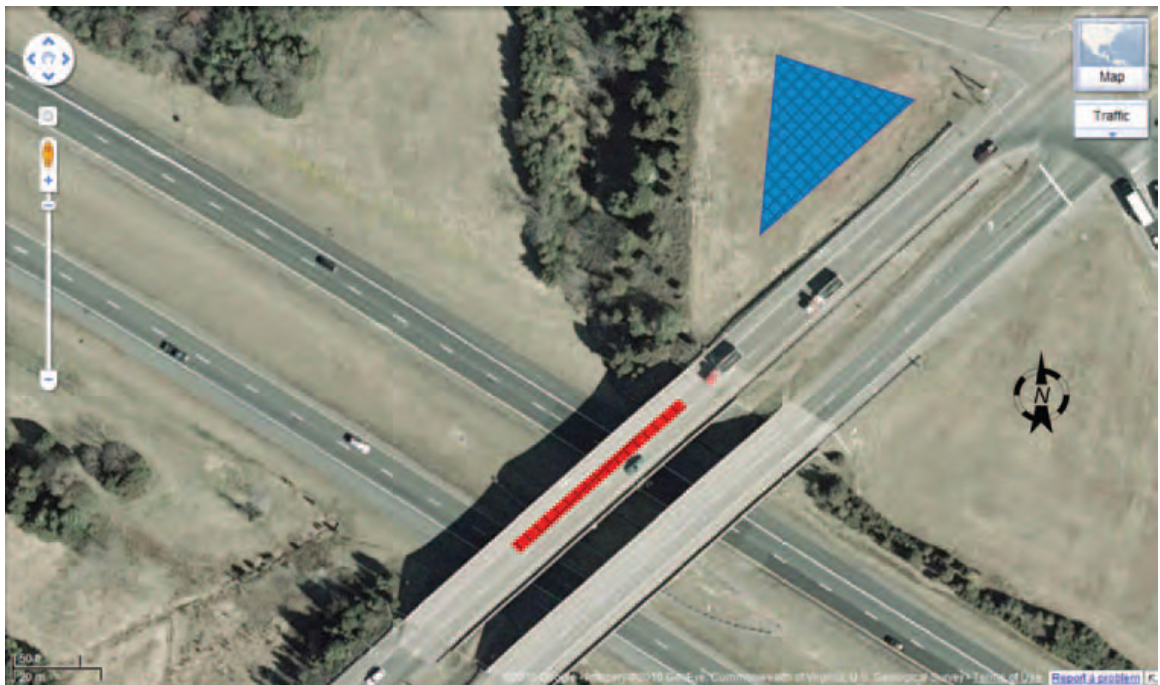


Figure 22: Route 15 bridge over I-66 in Haymarket, Virginia.

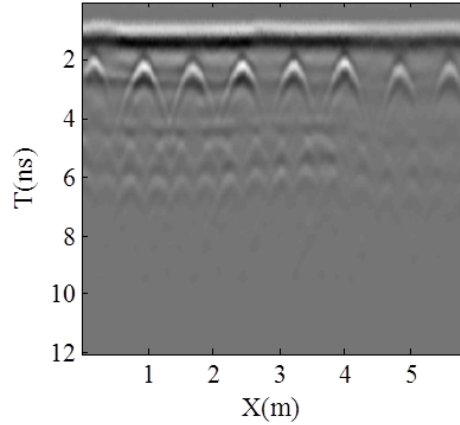


Figure 23: The original GPR profile collected from the real bridge deck.

3.3.2 Results and Discussions

For the experimental data, the resulted profiles from both BS method and F-K filtering are shown in Figure 24(a) and 24(b), respectively. For an experimental case, the roughness of the surface and the inhomogeneity of the medium are inevitable for concrete bridge decks. From Figure 24(a), it can be observed that strong direct wave and cross bar signal residues still exist in the profile after applying the BS method while the interferences are largely reduced by the F-K filtering with adequate dip relaxation. The results after F-K filtering with no dip relaxation and non-adequate relaxation are also shown in Figure 24(c) and 24(d), respectively. Figure 24(c) generates similar results as that after BS. Figure 24(d) indicates that if the selected dip angle is too small, the resulted profile may still have a large amount of interference residues. Another thing worth noticing is that the direct waves look flat from visual inspection in Figure 21, but it is actually not. The experimental results show that the F-K filtering with appropriate dip relaxation is more effective to remove uneven crossing rebar signals and direct waves. Similar conclusions can be drawn from the field testing results, which are shown in Figure 25. Since the field data is more challenging than the experimental data, the advantages of F-K filtering with appropriate dip relaxation are more obvious. The appropriate dip relaxation value is determined

empirically. For both the experimental and field data in the thesis, the upper limit of the dip relaxation is 10 degrees.

To show the impact of the proposed interference removal method and background subtraction on the performance of autofocusing techniques presented previously, the variations of NMV for HOT with the change of RDP are plotted in Figure 26 for the leftmost rebar in Figure 21. The desired autofocusing metric performance is that the metric should reach a single maximum value around the real relative permittivity value. The results show that, after F-K filtering with adequate dip relaxation, the performance of HOT is greatly improved compared with that after background subtraction.

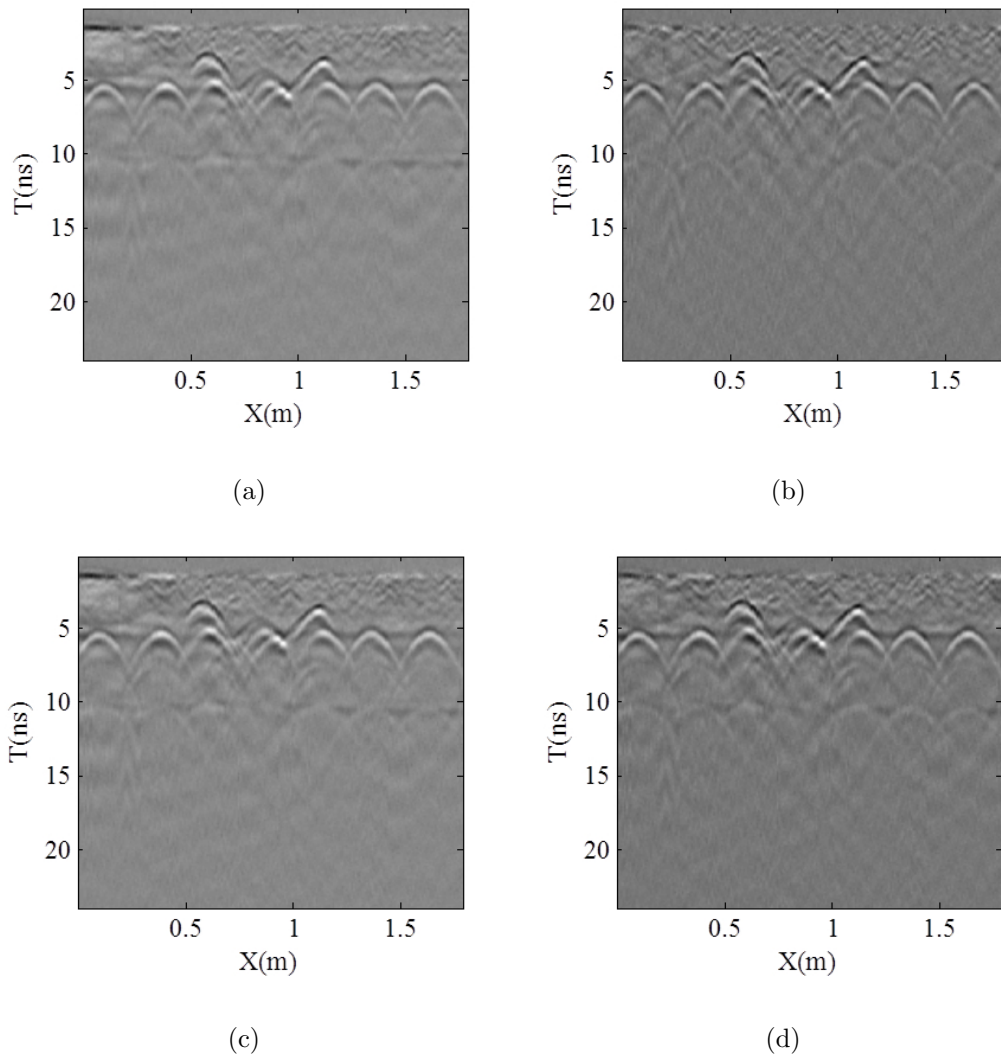


Figure 24: The experimental GPR profiles after (a) BS, and F-K filtering with (b) adequate dip relaxation, (c) no dip relaxation, (d) non-adequate dip relaxation.

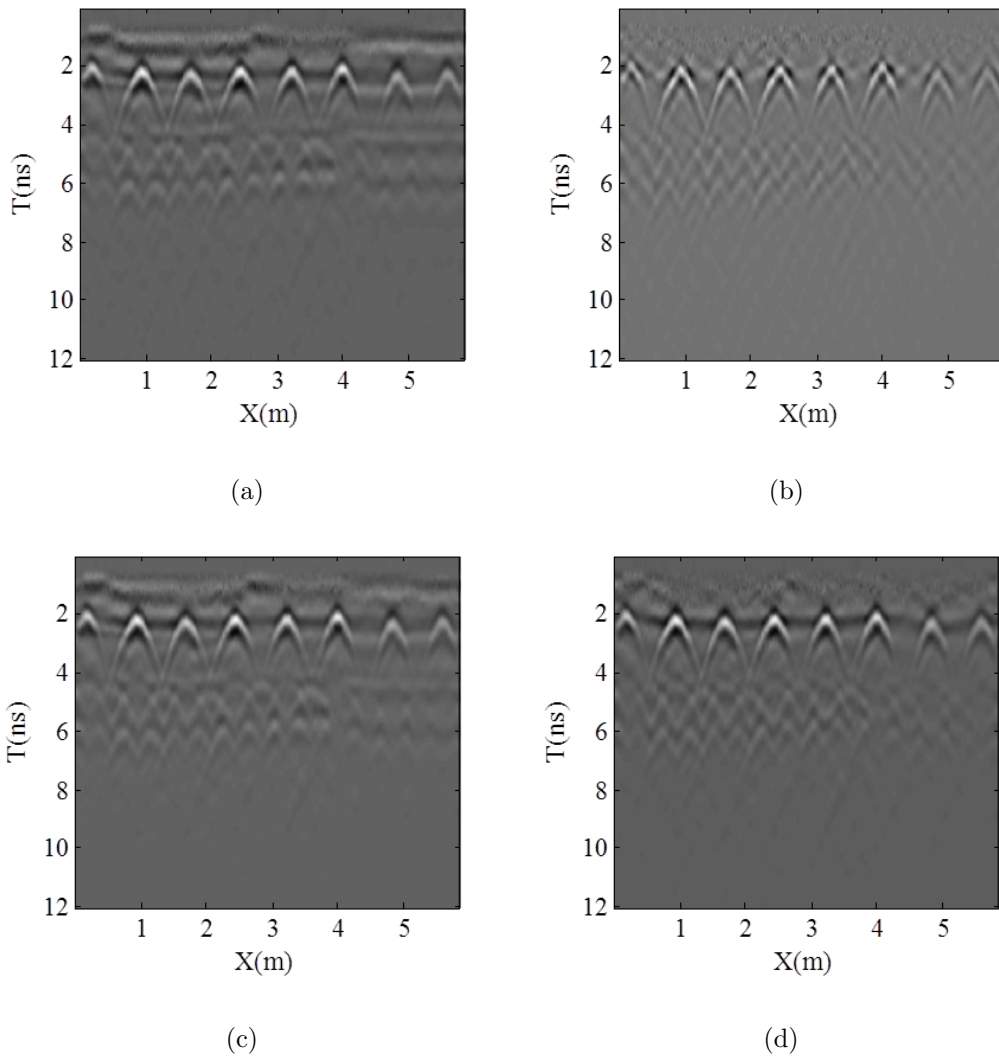


Figure 25: The field GPR profiles after (a) BS, and F-K filtering with (b) adequate dip relaxation, (c) no dip relaxation, and (d) non-adequate dip relaxation.

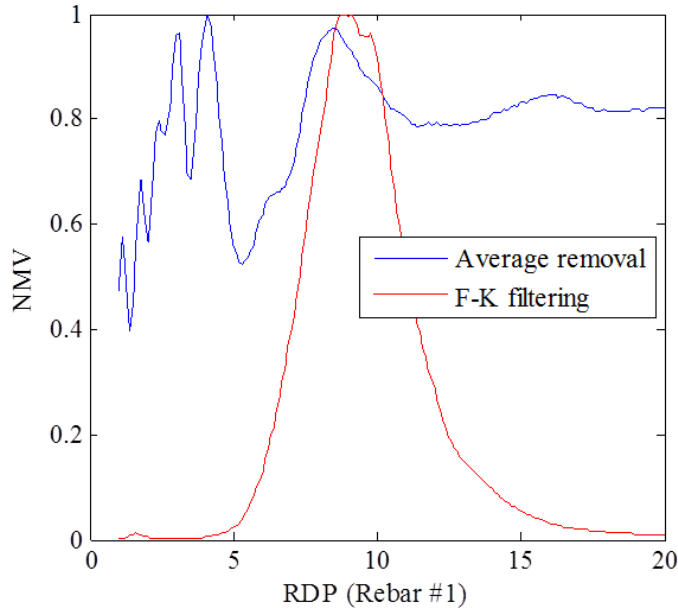


Figure 26: Performance comparison of HOT for preprocessed data after BS and F-K filtering.

3.4 Summary

In this chapter, an interference removal method based on F-K filtering is introduced to remove strong direct waves and cross rebar reflections under unfavorable environments in order to improve the GPR imaging and post-processing performance, such as autofocusing and the CS-based migration. Different from the previous work, Dip relaxation is introduced into the design of the F-K filter to accommodate surface roughness and medium inhomogeneous encountered in real RC bridge decks. For direct waves, rough surface is modeled as reflectors with small dipping angles. For straight crossing rebars in inhomogeneous medium, the rebar reflections exhibits as rugged line-like signals in the GPR profile. In this way, cross rebars in inhomogeneous medium can be modeled as rugged cross rebars in homogeneous medium and they share similar properties as the rough surface. Both experimental and field study show that interferences can be better removed by F-K filtering with dip relaxation as compared to standard methods.

CHAPTER IV

MODIFIED CS-BASED MIGRATION

4.1 Theory of CS-Based Migration

In the previous work, the ray tracing theory is adopted to build a relationship between the traditional measurements and the target space. The unknown vector, x , represents the discretized target space grids lined up as an array. A non-zero element in x suggests the target existence in the corresponding grid. For the scan position i , a dictionary, Ψ_i , is built with the j th column as the response of a point-like target in the j th discretized grid of the target space, which is the source signal scaled and delayed by the wave propagation time

$$\psi_j(t) = \frac{\sigma_j r(t - \tau_i(j))}{a_{\{i,j\}}}, \quad (22)$$

where r is the source signal, $\tau_i(j)$ is the round-trip delay between the transceivers at the i th scan point and the target is in grid j , σ_j is the reflection coefficient of the target and $a_{\{i,j\}}$ is a scaling factor to account for any attenuation and spreading losses. However, as $a_{\{i,j\}}$ is usually unknown, it is simplified as

$$\psi_j(t) = r(t - \tau_i(j)). \quad (23)$$

In this way, x is a weighted indicator vector defining the target space, i.e., if there is a target at the j th grid, the value of the j th element of x will be $\sigma_j/a_{\{i,j\}}$, otherwise, it is zero. The traditional measurement vector for scan position i , ζ_i , can be represented by $\Psi_i x$. After establishing the relationship $\zeta_i = \Psi_i x$, a random projection needs to be performed by multiplying both sides of the equation with the CS measurement matrix, Φ_i . This is done for all the scan positions, then ζ_i , Φ_i and Ψ_i are stacked vertically to construct the final ζ , Φ and Ψ .

The required number of compressive measurements to reconstruct the target space exactly with high probability is $C(\mu^2(\Phi, \Psi)\log N)K$, where C is usually a small constant and $\mu(\Phi, \Psi)$ is the mutual coherence between Φ and Ψ . Six CS measurement matrices in the previous work are briefly introduced as follows [34]. Type I is constructed of entries drawn from $N(0, 1)$, Type II is constructed of random ± 1 entries with probability of 0.5, Type III matrix is constructed by randomly selecting some rows of an identity matrix, which is equivalent to measuring random space-time domain samples, Type IV, V, and VI are random matrices that lie between Type II and III by selecting a random subset of the data at each scan point and projecting the data subset onto vectors having random ± 1 entries with probability of 0.5 (Type IV uses 50% of the data, Type V 10%, and Type VI 2%). Different CS measurement matrices will affect both the required number of CS measurements and the hardware realization.

Finally the problem for GPR imaging is formulated as solving a l_1 minimization problem:

$$\hat{x} = \arg \min \|x\|_1 \quad s.t. \quad y = \Phi\zeta = \Phi\Psi x = Ax. \quad (24)$$

Due to the modeling errors and the ubiquitous noise in real environments, a stable recovery of the sparse unknown vector, x , is possible by solving the following relaxed l_1 convex optimization problem, called the Dantzig Selector [17]:

$$\hat{x} = \arg \min \|x\|_1 \quad s.t. \quad \|A^T(y - Ax)\|_\infty < \varepsilon_1. \quad (25)$$

Another possible solution can be constraining the l_2 -norm of the measurement error:

$$\hat{x} = \arg \min \|x\|_1 \quad s.t. \quad \|y - Ax\|_2 < \varepsilon_2. \quad (26)$$

ε_1 and ε_2 are the regularization parameters. Generally, a higher value of the regularization parameter will miss some targets while a lower value will take significant portions of the noise as target signals and it is stated that if the noise statistics are

known, a "good" choice can be made. However, the statistics of the modeling errors and other noise in real cases are very difficult to be formulated. The selection of the regularization parameters in this thesis is based on visual inspections and our investigation also discovered that this parameter will also impact the results in the aspects of comparative amplitude preservation and the image clarity. The second l_1 minimization formulation is favored as it is a linear problem and easier to implement as compared to the minimization problem in the third, which is a second-order cone problem [14]. The problems in this paper are solved using l_1 -magic, a convex optimization package developed by [3].

4.2 *Waveform Distortion Mechanisms*

The impulse sent out by time-domain GPRs is generally characterized by narrow support in time and wide support in frequency. The wave propagation in the previous work is simplified that there is no waveform distortion during the wave propagation process. However, due to factors, such as wave propagation medium and the geometrical structure of the target, the amplitude and phase responses with respect to different frequencies varies. A waveform distortion can be resulted when this phenomenon gets severe. Impulse distortion can be observed in the GPR data collected from RC bridge decks, and the waveform corresponding to the rebar reflection no longer follow the shape of the standard exciting source, e.g., the commonly used Ricker function. Therefore, a more precise model accounting the waveform distortion phenomenon needs to be built.

The frequency dependence can be considered from both aspects of the amplitude and the phase that is equivalent to the delay. A generalized model can be formulated as

$$\Psi_i(t) = \int A(\omega)R(\omega) \exp(j\omega(t - \tau_i(\omega)))d\omega, \quad (27)$$

and

$$R(\omega) = \int r(t) \exp(-j\omega t) dt, \quad (28)$$

where $r(t)$ represents the incident impulse, ω represents the angular frequency, A represents the frequency-dependent scaling, and τ represents a frequency-dependent shift parameter.

Exact frequency-dependent information embracing all factors is difficult to obtain if possible. However, there are still ways around it. For example, antenna response and medium dispersion can be measured in advance. The scatter effect is also studied in the literature. For example, the first-order geometrical theory of diffraction (GTD) [26][7] illustrates an edge, endpoint, and finite smooth surface contribute frequency dependencies proportional to $\omega^{-1/2}$, $1/\omega$, and ω , respectively. One thing needs to be kept in mind is that the solving of scattering problem can be highly susceptible to improper modeling and model-order selection [49][41]. For simplification, the formulation of the waveform distortion considering only this effect can be

$$\Psi_i(t, \alpha) = \int [\omega \exp(j\pi/2)]^\alpha R(\omega) \exp(j\omega(t - \tau)) d\omega. \quad (29)$$

Positive integers α corresponds to α differentiations of the incident field, whereas negative integers α correspond to α integrations. Integer values of α for the context of underwater scattering is used in [6] and the dictionary is augmented to $\{0, \pm 1/2, \pm 1, \pm 3/2, \pm 2, \pm 5/2\}$ by including functions that correspond to single and multiple edge diffractions in [49]. It is also stated that each α corresponds to a possible diffraction mechanism, and more α could be included if desired [49].

Building an over-complete dictionary considering all possible factors is challenging and the point to point measurements of the factors such as permittivity variation with frequency is difficult and time consuming for bridge deck probing. For our application, the simplified formulation has been tested to be enough. An example of the real part of the concrete permittivity is provided in [57], which shows the waveform dilation

caused by medium dispersion can be neglected as the resulted waveform dilation is minor. However, for applications where severely dilated waveforms are resulted, this factor should be taken into consideration. Accurate modeling produces less modeling errors and it is even more beneficial when the original images need to be recovered. The obtained factor, α , can also be used to deduce the shape of the scatter for certain applications.

The wave propagation mechanisms introduced above can be incorporated into the CS model by building a super dictionary. However, it may greatly increase the size of the problem and the computational complexity. As the targets in this application are uniformly distributed standard-sized rebars at the same depth, matching pursuit [47][82] is recommended to capture a reference waveform as a replacement of the source waveform in the previous CS dictionary.

4.3 Simulation Study

4.3.1 Direct Waves

The simulation setups are basically the same as previous. Direct waves and random background noise are two major factors that pollute GPR images. The previous work has already studied the effect of the additive Gaussian random noise on the performance of the CS-based migration and the comparison is made with a traditional migration technique, time-domain standard backprojection (SBP). For low SNR, the traditional migration provides better results than CS-based migration while CS-based migration provides better results for cases with high SNR. Here we are not going to duplicate results on the effect for random noise, but are more focused on the effects of direct waves. The data is first downsampled by 2 spatially to be well better handled by commonly available computers.

The CS measurement matrix adopted in this chapter is Type I random matrix and its entries are drawn from $N(0, 1)$. It has been reported to lead to a small coherence,

which means less CS measurement data are required to recover the unknowns. The number of the CS measurements in this chapter is 20. The CS measurement matrix is kept the same for all scan positions for the purposes of the reduction of the memory requirements and the simplification of implementation. In addition, using different measurement matrices for each scan position do not provide better results for most cases here.

Figure 27(a) shows the original GPR data for the simulated RC bridge deck with a single rebar placed at 1.2 m along the x-axis and at a depth of 2.5 in.. Figure 27(b) shows its preprocessed data. Figure 28(a) and 28(b) show examples of the results of CS-based migration with a low value of the regularization parameter and a high value of the regularization parameter, respectively. Figure 28(c) shows the results of the F-K migration. Figure 29(a) and 29(b) show an example of results of CS-based migration and F-K migration on the preprocessed data, respectively. It can be observed that, under the interference of strong direct waves, CS-based migration may fail to recover the target information while traditional F-K migration can still provide correct information about the target. The probability to recover the target signals under the pollution of strong direct waves is quite low. A Monte Carlo simulation using 100 trials is performed and each trial uses a different CS measurement matrix. Only 20 out of 100 can successfully recover the target signals with the pollution of direct waves while 100 out 100 can successfully recover the target signals without the pollution. The reason may be that the direct wave formulation severely violates the ray-tracing model built for point-like targets. For the strong ground bounce caused by the air-concrete interface, the target can be considered as a line-like target. Even if it can be considered as multiple point-like targets, it violates the prerequisite of the sparsity and the assumption that the targets do not interact, and hence the superposition is not valid. The crosstalk does not follow the ray-tracing model built for the point-like targets, either. Although its formulation mechanism is different, it

can be generally considered as ground bounce reflected from an absolute flat metal plate for the problem concerned here. For RC bridge decks, cross rebar signals also share similar properties as ground bounce. Therefore, the successful elimination of interferences, such as direct waves and cross rebar signals, is much more important for CS-based migration than traditional F-K migration.

For ideal situations when the surface is flat, the targets are deep enough, and the medium is homogeneous, simple direct wave removing methods such as time gating, average removal, and scale and shift can be adopted. However, when GPR scans are collected on rough surfaces for shallow targets or close to the cross rebars buried in comparatively inhomogeneous concrete, the removing of the direct waves and cross rebar signals become more challenging, then sophisticated methods should be adopted. The interference removal is discussed in more detail in the previous chapter.

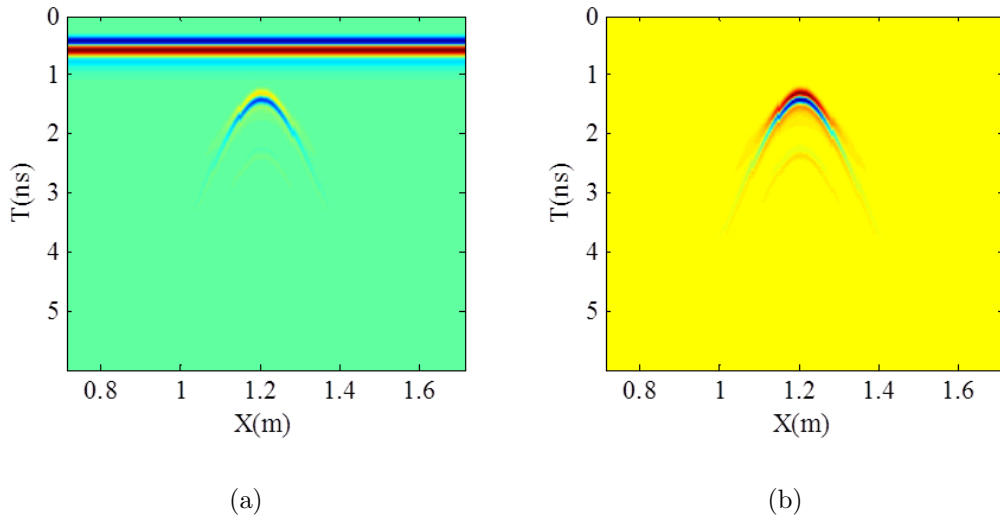
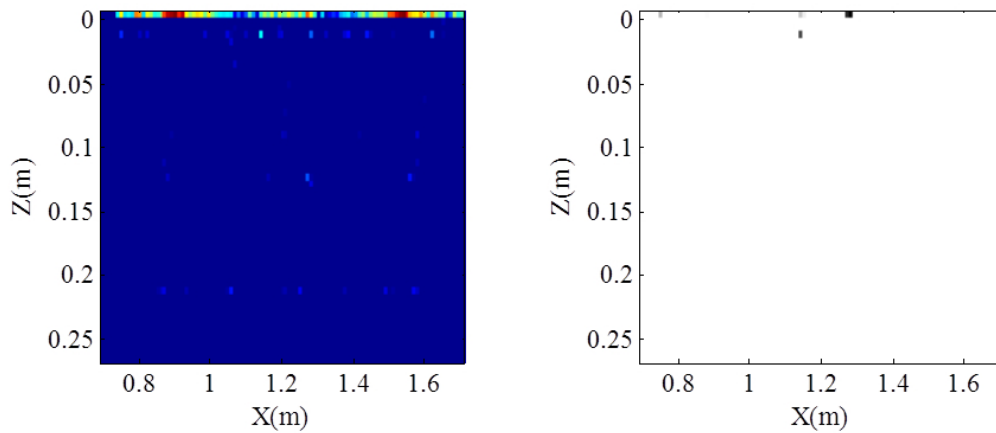
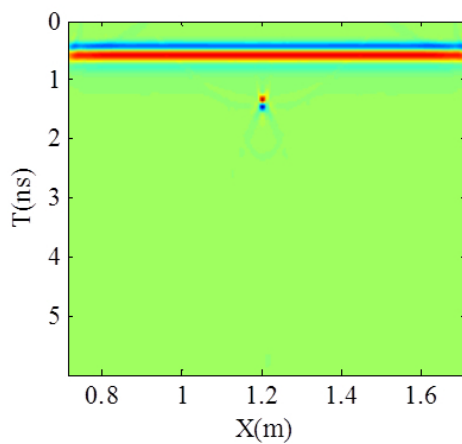


Figure 27: Simulated GPR profiles of (a) the original data and (b) the preprocessed data.



(a)

(b)



(c)

Figure 28: Results of (a) CS-based migration with a low regularization parameter, (b) CS-based migration with a high regularization parameter, and (c) F-K migration on the original GPR data.

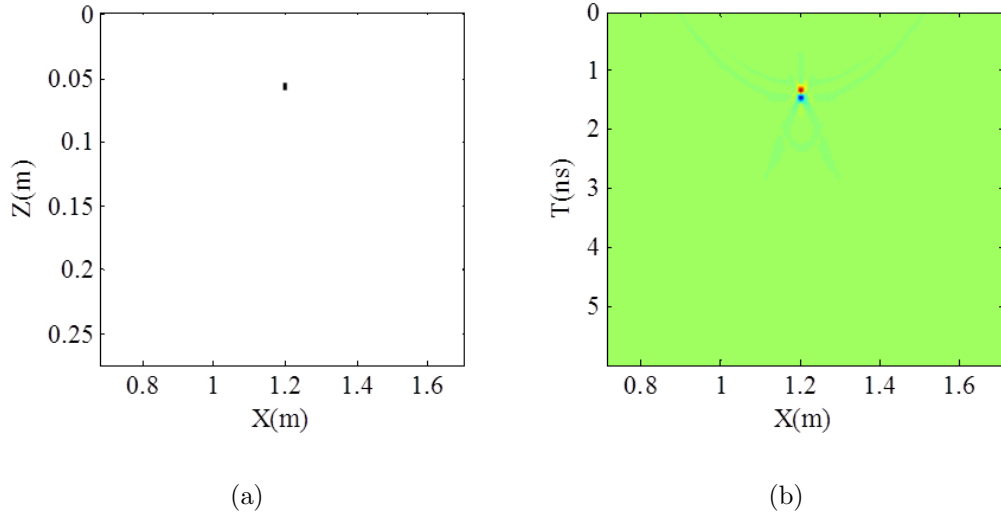


Figure 29: Results of (a) CS-based migration and (b) F-K migration on the preprocessed GPR data.

4.3.2 Waveform Distortion

The upper figure of Figure 30 shows the rebar reflection signal from a GPR A-scan collected on the simulated bridge deck described above. It can be observed that the rebar reflection is a distorted wavelet, compared to the source signal. The results from the matching pursuit indicate 0.5 as the value for α best fit the distorted waveform, which is shown in red and overlapped very well on the rebar reflection in blue in the lower figure of Figure 30. The results from the original model are shown in Figure 31(a) and the results from the improved model are shown in Figure 31(b) when all other parameters are kept the same. It is shown that the modified model provides better results. If the same performance needs to be achieved for the previous model, a higher value of the regularization parameter is needed as more modeling noise are produced. For applications when the original images needs to be recovered, this problem may become even more important.

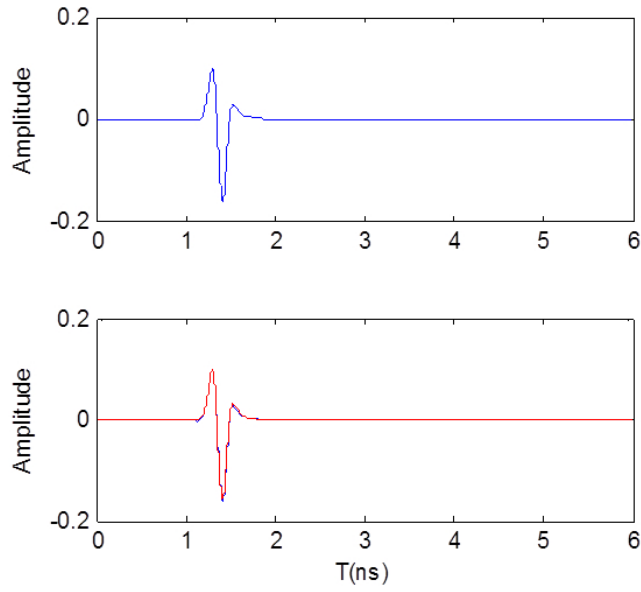


Figure 30: Rebar reflection and the best matching dictionary element.

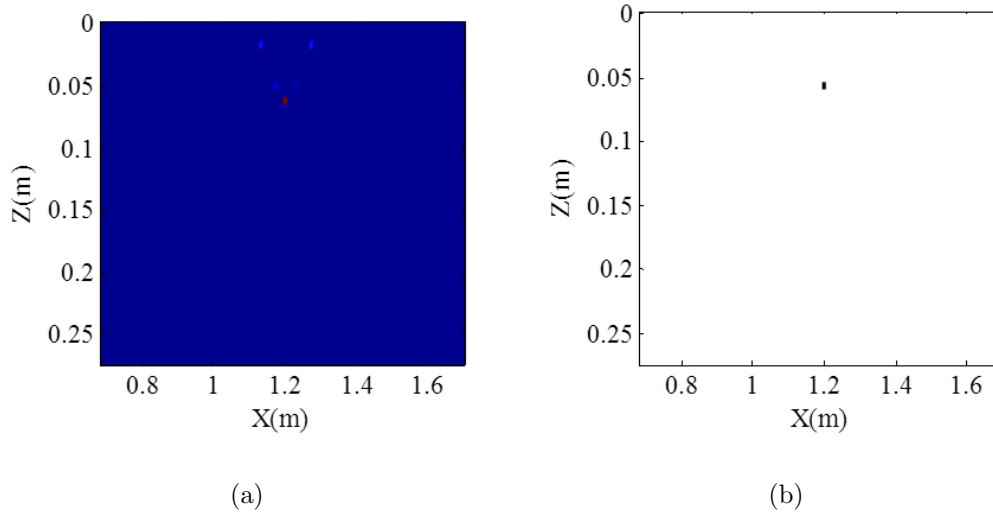


Figure 31: CS-based migration with (a) the previous model and (b) the modified model.

4.3.3 Comparative Amplitude Preservation

The attenuation map is an important tool for the health condition evaluation of RC bridge decks, such as concrete degradation and rebar corrosion. Whether or not CS-based migration can well preserve the comparative amplitude information of the rebar

reflections may affect its popularity in this application. Investigation shows that if the GPR profile with multiple rebars are processed at one time by CS-based migration, the comparative amplitude information cannot be preserved while maintaining a clear image at the same time. An example is shown using the simulation model with three rebars buried at 1.0 m, 1.2 m, and 1.4 m, respectively, along the x-axis. Figure 32(a) shows the original GPR profile and Figure 32(b) is the preprocessed profile. Figure 33(a) and 33(b) show the results of the CS-based migration with a high regularization parameter and a low regularization parameter, respectively. For a high regularization parameter, a clear image can be obtained, but the amplitudes of the rebar reflections varies significantly from each other. For a low regularization parameter, the image can be heavily cluttered, but the comparative amplitude reservation is better. Various regularization parameters with high density are attempted, it is hardly possible to find a regularization parameter to generate a clear image and at same time preserve the comparative amplitude information. The reason for the variation of the amplitude in the rebar reflections is not known and a possible reason is model mismatch. The investigation of the very reason can be the future work. For comparison, the results of the F-K migration is shown in Figure 33(c), where the comparative amplitude information is well preserved.

A simple approach is proposed to preserve the comparative amplitude information and at the same time maintain the clarity of the image. Different from other applications, the rebar spacing can be prior information and the rough idea of the rebar positions can be deduced when the initial rebar is localized, which make segmentation according to each rebar possible. There are other issues when migrating the whole B-scan at one time using CS-based migration. For example, the computational cost and memory requirement can be greatly reduced. The convex optimization programs use interior point methods that iterate Newton's method. For the optimization of the l_1 minimization problem here, the computational cost is $O(n^3)$ with observably

low iterations that is almost independent of the size of the problem [34]. The computational cost increase dramatically with the increase of the target space grids for the same resolution. Another aspect is that, for cases when the large scale medium homogeneity is invalid, the ray-tracing model becomes difficult to apply for the entire profile and segmentation can also help achieve better implementation when the assumption of local homogeneity still holds.

Figure 34 shows the results of the proposed method on the same dataset and it demonstrates the proposed method can not only recover all the rebars accurately, but also preserve the amplitude information successfully. When the rebar spacing is not the integral multiples of the scan step, which means the the relative position of the antennas and the target are not the same for each rebar, the comparative amplitude reservation is also investigated here with an example of the rebar spacing is 20.2 cm. The results, shown in Figure 35, demonstrates that the proposed approach can still reserve the comparative amplitude reservation in this case.

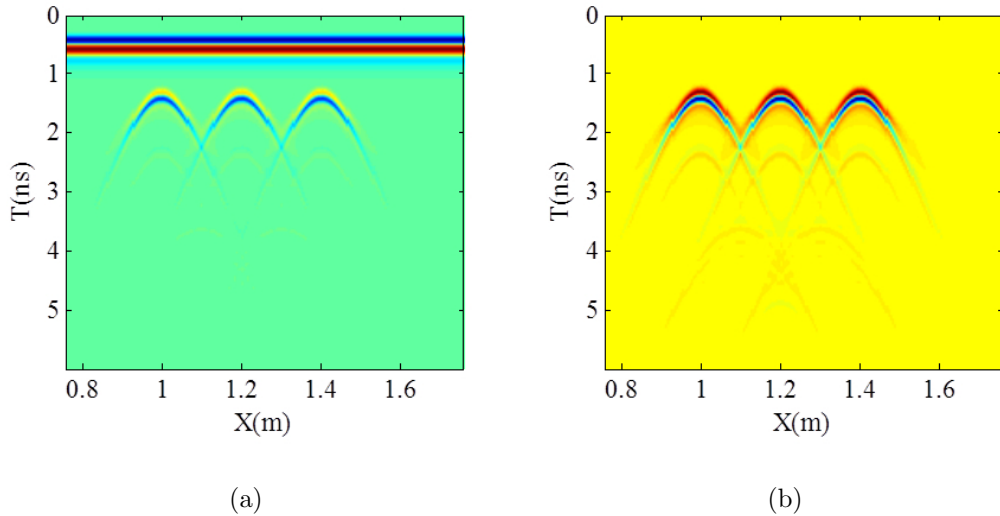
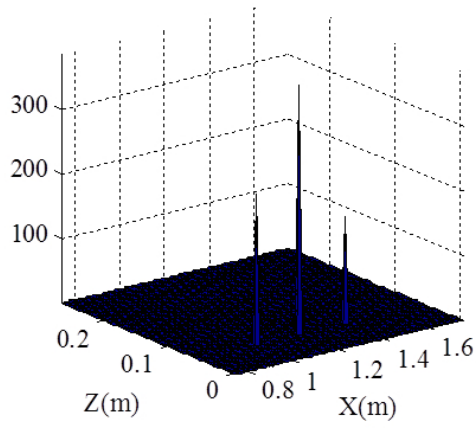
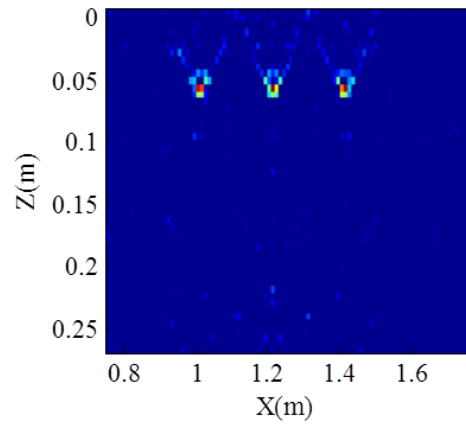


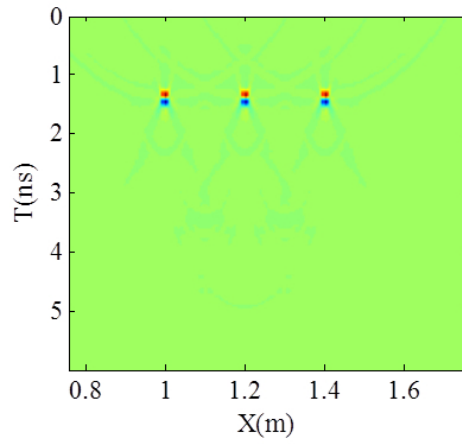
Figure 32: (a) The original GPR profile and (b) preprocessed GPR profile for multiple rebars.



(a)



(b)



(c)

Figure 33: (a) CS-based migration results with a high regularization parameter and (b) with a low regularization parameter, and (c) F-K migration results for the preprocessed GPR profile with multiple rebars.

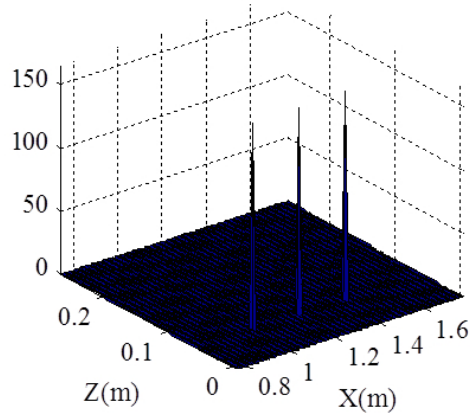


Figure 34: The results of the proposed amplitude reservation method for multiple rebars when the rebar spacing is integral multiples of the scan step.

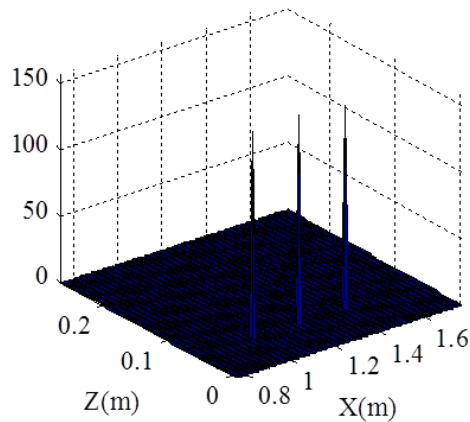


Figure 35: The results of the proposed amplitude reservation method for multiple rebars when the rebar spacing is not integral multiples of the scan step.

4.3.4 Uniform Downsampling

For time-domain GPR systems, the data acquisition time for a fixed scan position cannot be reduced by CS measurements. The data acquisition time can be reduced by decrease the scan points only through Type III CS measurements mentioned above. As Type III CS measurements are basically a random selection of the scan positions, it may place risks on the recovery of certain targets if scans with strong target

information are skipped, shown in Figure 9(a) in [34]. In addition, the hardware realization of the CS measurements can be challenging for the current commercial GPR systems. Uniform sampling from both dimensions with sampling rates less than the requirements for traditional migration techniques (we call this process uniform downsampling for simplification here) and then followed up by the CS-based migration are evaluated here.

The reduced uniform sampling rate for a fixed scan position suggests a smaller size of directly sampled data. An example is shown here. Figure 36 shows the downsampled GPR profile and Figure 37(a) and 37(b) are the results from CS-based migration and the F-K migration, respectively, with a temporal uniform downsampling rate of 70 from the original setup, which is equivalent to 2.6 times less samples than that required by the Nyquist sampling rate. The CS-based migration is not affected by the reduced uniform sampling rate while F-K migration generates unfocused fuzzy image around the location of the target. The reason for this is that the reduced sampling rate is lower than the Nyquist sampling rate required by F-K migration. The center frequency of the exciting source is 2.6 GHz and the highest frequency needs to be taken into consideration is approximately three times the center frequency, which is 7.8 GHz. Thus the Nyquist sampling frequency here is 15.6 GHz. The sampling frequency for a uniform downsampling rate of 30 is 14.1 GHz, which is lower than the Nyquist sampling rate for traditional migration techniques. The sampling rates for a downsampling rate of 70 (the sampling frequency will be 6.1 GHz) will be even lower than the required Nyquist sampling rate. To test how much the sampling rate can be reduced, the probability of recovery (POR) with respect to the down sampling rates is investigated. If the correct location of the target is recovered without any clutter, the recovery is considered successful. For each downsampling rate, the CS-based migration is run 50 times and the POR with changing down sampling rates is shown in Figure 38.

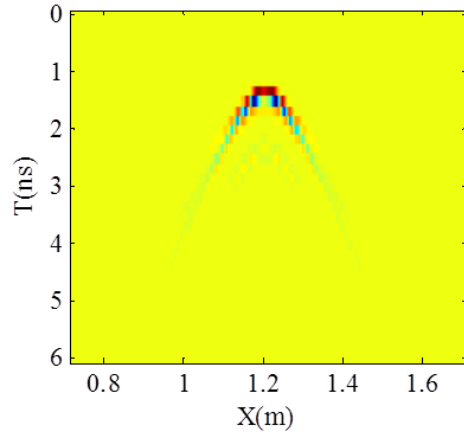


Figure 36: The downsampled GPR profile for temporal downsampling rate of 70.

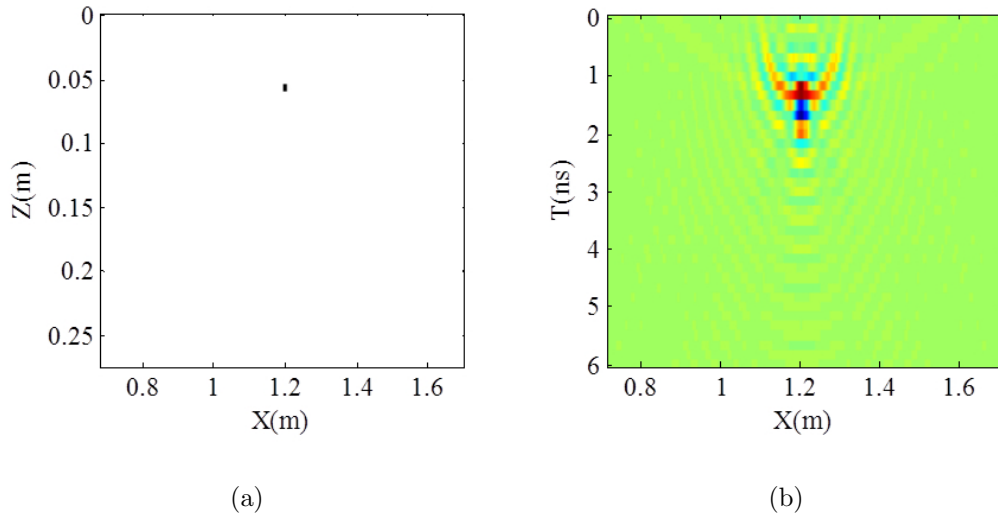


Figure 37: (a) CS-based migration and (b) F-K migration results for temporal downsampling rate of 70.

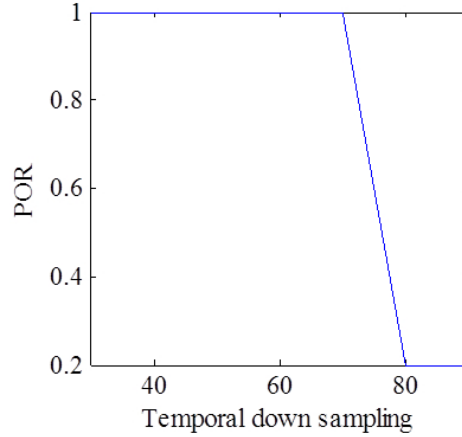


Figure 38: POR with various temporal downsampling rates.

The reduced number of scan points suggests faster data acquisition speed and smaller data size. Figure 39 is GPR profile after downsampling and Figure 40 show the results of CS-based migration and the results of F-K migration for the spatial downsampling rate of 6, which is approximately 4 times less than that required by traditional migration method. It can be observed that CS-based migration can still provide clear accurate high-resolution images using less scan points along the spatial domain while Stolt F-K migration failed. The Spatial aliasing is a practical issue associated with 2D Fourier transform for Stolt F-K migration [32]. The required scan step according to this rule is at most 7.6 mm here. A spatial down sampling of 2 will lead a scan step of 10 mm, which is larger than the required scan step. The POR with changing spatial down sampling rate is shown in Figure 41. For the case when the rebar spacing is not the integral multiples of the scan step, an example of spatial downsampling of 2 is shown in Figure 42 and the comparative amplitude information can still be well preserved. However, a slightly larger deviation will occur in this case when the downsampling is larger than 3. Although the uniform downsampling rates are not that significant, it is still very meaningful to this application. For example, if the data acquisition speed of a vehicle mounted GPR system is 15 miles an hour, an increase by four times will push it to the traffic speed on a highway.

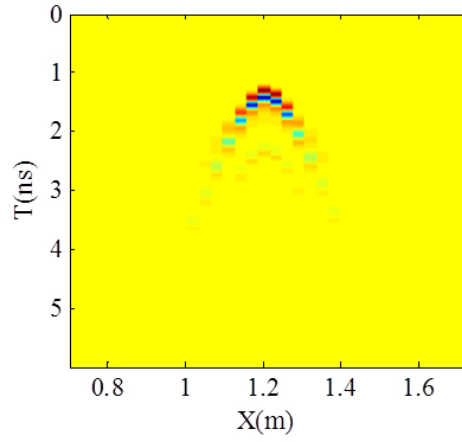


Figure 39: The downsampled GPR profile for spatial downsampling rate of 6.

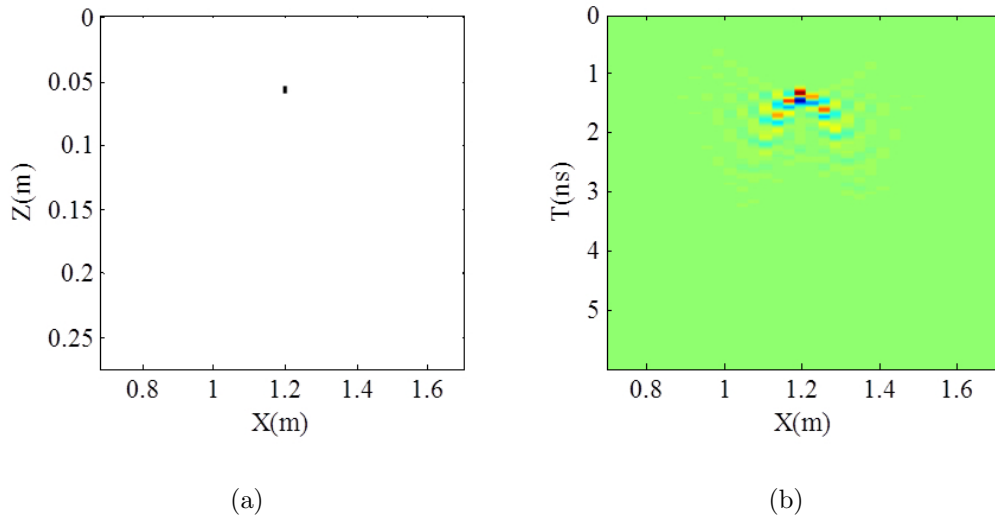


Figure 40: (a) CS-based migration and F-K migration results for spatial downsampling rate of 6.

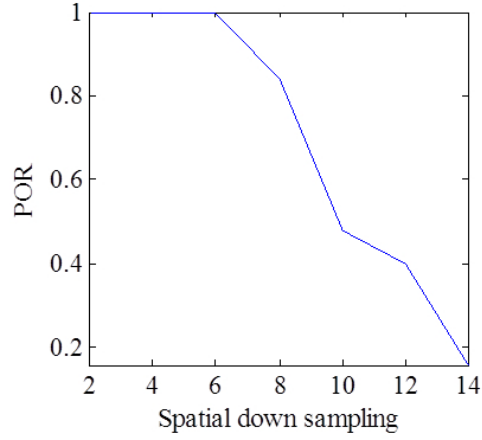


Figure 41: ROR with various spatial downsampling rates.

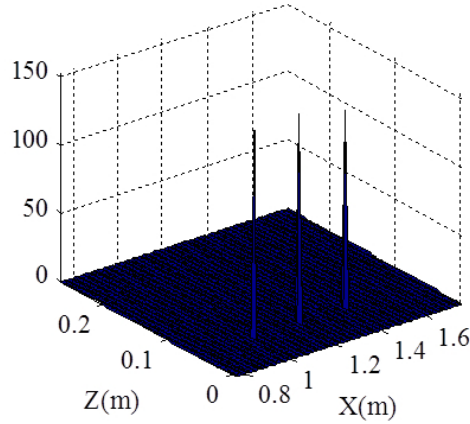


Figure 42: The results of the proposed amplitude reservation method for multiple rebars when the rebar spacing is not integral multiples of the scan step (down sampling rate is 2).

4.4 *Experimental Demonstration*

The experimental data is collected along the vertical line at 0.68 (2.25 ft.) along the horizontal axis. Figure 43(a) and 43(b) shows that original GPR profile and the pre-processed version, respectively. A segmented image for the rebar on the left is shown in Figure 44. The results from the CS-based migration are shown in Figure 45(a), which is a high-resolution image with much less clutter compared to the results from the traditional migration method, shown in Figure 45(b). Both migration techniques

failed to successfully recover the rebar information on the second layer because the rebar reflections from the second layer are almost noise level. An approach to extract the signals from rebars on the second layer is proposed in [79][77].

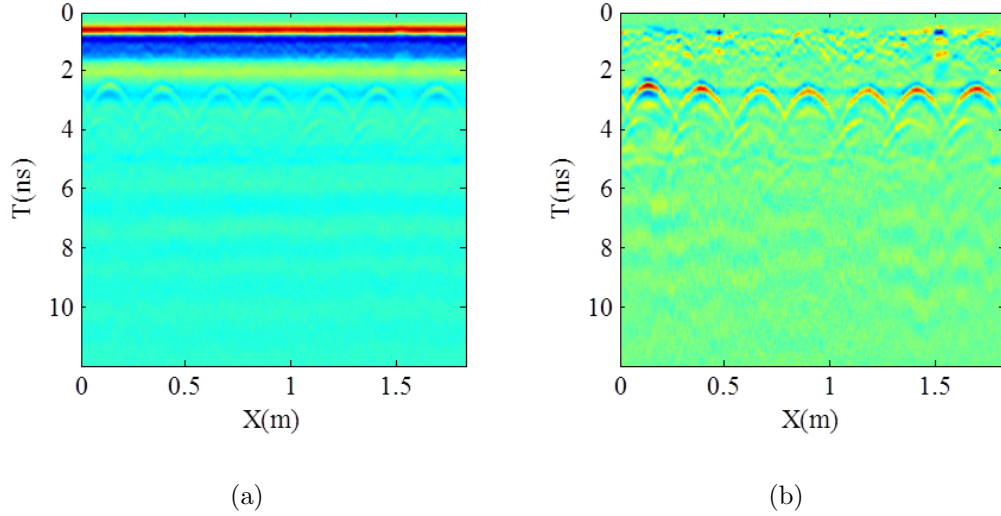


Figure 43: Original GPR profile and the preprocessed GPR profile for the experimental data.

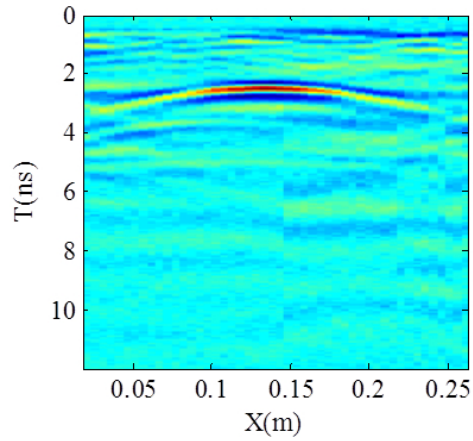


Figure 44: Segmented GPR profile for the leftmost rebar.

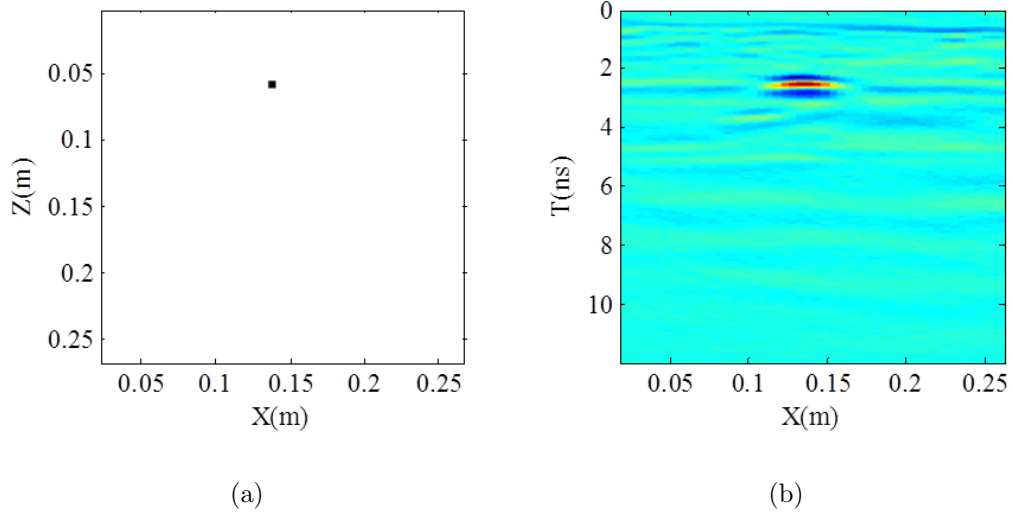


Figure 45: Results of (a) CS-based migration and (b) F-K migration.

4.5 Summary

CS-based migration has been applied in GPR imaging recently. The major benefits are to generate high-resolution images with less clutter using a small number of CS measurements when the target space is sparse. The work in this chapter improved the previous work in two aspects. First, a more accurate model accounting for the waveform distortion is built and less modeling error is resulted. Second, segmentation according to each rebar and then implementing CS-based migration separately is proposed to preserve the relative amplitude information of the rebar reflections while still maintaining a clear image at the same time. The proposed approach can also greatly reduce the computational complexity and memory requirement. In addition, the uniform downsampling from both directions is investigated for the purposes of reduced number of directly measured data and data acquisition time. Although the allowed reduction rate is not significant, it is still valuable for this application.

CHAPTER V

CONCLUSION

5.1 Dissertation Contribution

In this thesis, autofocusing, interference removal, and modified CS-based migration are presented. The contributions are list as follows.

First, multiple autofocusing metrics are introduced to replace the expensive and less reliable human visual inspections during the iterative process of the medium velocity distribution estimation. The effectiveness of the metrics is evaluated with respect to potential deterioration factors, namely, noise, synthetic aperture width, and cross rebar reflection interference, on the simulation data. Among the proposed candidates, high-order statistics demonstrate the best performance in terms of robustness and sensitivity. Conclusions drawn from the simulation study are also validated by the experimental data.

Second, F-K filtering with dip relaxation is proposed to remove direct waves and cross rebar reflections under rough environments, such as uneven surface and inhomogeneous medium. The principle of the F-K filtering is illustrated by simulation data. The effectiveness of the proposed approach is evaluated by both experimental and field data. Results show that the proposed method can better remove the interferences as compared to the standard direct wave removing method.

Third, the previous CS-based migration is modified on two aspects. First, a more accurate model accommodating the waveform distortion is built and less modeling error is resulted. Second, as it is hardly possible to obtain a regularization parameter to preserve the amplitude information and at the same time maintain the image clarity,

a simple trick based on segmentation according to each rebar is proposed and validated. The proposed approach can also help greatly reduce the computational cost and memory requirement. In addition, uniform downsampling is investigated generally for less directly sampled data. Uniform downsampling along the spatial direction also helps increase the data acquisition speed. Although the allowed downsampling rates are not significant, it can still be valuable for this application.

5.2 *Future Work*

In this section, potential future work related to each of the topics studied in this thesis are presented.

First, for the optimized maintenance of RC bridge deck under a tight budget, the accuracy and resolution of the RDP distribution provided by the method proposed is generally sufficient. However, if RDP values with higher accuracy are required, accurate modeling with less unpractical assumptions, such as circular wavefront, accurate determination of the time-zero, or experimental calibration may help improve the results.

Second, for F-K filtering with dip relaxation, the threshold of dip relaxation is currently manually obtained. A possible approach to obtain the dip relaxation threshold automatically can be to extract the largest slope in the interference structures of the original GPR profile using image processing techniques.

Third, for the modified CS-based migration, more careful study of the waveform distortion mechanisms can be pursued; the very reason why the comparative amplitude information cannot be well preserved when the GPR profile with multiple rebars is processed by CS-based migration at one time can be further investigated.

REFERENCES

- [1] www.fhwa.dot.gov/bridge/nbi/defbr10.cfm#c.
- [2] <http://www.geophysical.com/>.
- [3] <http://www.cms.caltech.edu/l1magic/>.
- [4] AHMAD, F., AMIN, M. G., and MANDAPATI, G., “Autofocusing of through-the-wall radar imagery under unknown wall characteristics,” *IEEE Transactions on Image Processing*, vol. 16, no. 7, pp. 1785–1795, 2007.
- [5] AL-YAHYA, K., “Velocity analysis by iterative profile migration,” *Geophysics*, vol. 54, no. 6, pp. 718–729, 1989.
- [6] ALTES, R. A., “Sonar for generalized target description and its similarity to animal echolocation systems,” *The Journal of the Acoustical Society of America*, vol. 59, no. 1, pp. 97–105, 1976.
- [7] BALANIS, C. A., *Advanced Engineering Electromagnetics*. Wiley, 1989.
- [8] BARANIUK, R., “Compressive sensing,” *IEEE Signal Processing Magazine*, vol. 24, pp. 118–121, July 2007.
- [9] BARNES, L. C. and TROTTIER, F. J., “Phenomena and conditions in bridge decks that confound ground-penetrating radar,” *Transport Research Record*, vol. 1795, no. 1, pp. 57–61, 2002.
- [10] BARNES, L. C., TROTTIER, F. J., and FORGERON, D., “Improved concrete bridge deck evaluation using GPR by accounting for signal depth-amplitude effects,” *NDT&E International*, vol. 41, pp. 427–433, Mar. 2008.
- [11] BENTER, A., MOORE, W., and ANTOLOVICH, M., “Focusing ground penetrating radar images with vertical offset filtering,” *Progress In Electromagnetics Research*, vol. 19, pp. 183–195, 2011.
- [12] BERIZZI, F. and CORSINI, G., “Autofocusing of inverse synthetic aperture radar images using contrast optimization,” *IEEE Aerospace and Electronics Systems Magazine*, vol. 32, no. 3, pp. 1185–1191, 1996.
- [13] BLACK, J. and BRZOSTOWSKI, M., “Systematics of time-migration errors,” *Geophysics*, vol. 59, no. 9, pp. 1419–1434, 1994.
- [14] BOYD, S. and VANDENBERGHE, L., *Convex Optimization*. Cambridge University, 2004.

- [15] BROWN, J., NICHOLS, J., STEINBRONN, L., and BRADFORD, J., "Improved GPR interpretation through resolution of lateral velocity heterogeneity: Example from an archaeological site investigation," *Journal of Applied Geophysics*, vol. 68, no. 1, pp. 3–8, 2009.
- [16] BUYUKOZTURK, O., PARK, J., and AU, C., "Non-destructive evaluation of FRP-confined concrete using microwave," in *International Symposium on Non-Destructive Testing in Civil Engineering (NDT-CE)*, (Berlin, Germany), 2003.
- [17] CANDÉS, E. J. and WAKIN, M. B., "An introduction to compressive sampling," *IEEE Signal Processing Magazine*, vol. 25, pp. 21–30, Mar. 2008.
- [18] CHE, X., WANG, R., QIAO, W., CHEN, Q., CHENG, Q., LI, Y., ZHANG, T., and WANG, L., "A denoising method based on modified matrix pencil algorithm and F-K filter," in *5th International Congress on Image and Signal Processing (ICISP)*, pp. 1542–1545, 2012.
- [19] CLAERBOUT, J. F., *Imaging the Earths Interior*. Blackwell Scientific Publications, 1985.
- [20] COUNTS, T., GURBUZ, A. C., SCOTT, W. R., MCCLELLAN, J. H., and KIM, K., "Multistatic ground-penetrating radar experiments," *IEEE Transactions on Geoscience and Remote Sensing*, vol. 45, pp. 2544–2553, Aug. 2007.
- [21] DANIELS, D. J., *Ground Penetrating Radar*. Institution of Electrical Engineers, 2nd ed., 2004.
- [22] DONOHO, D. L., "Compressed sensing," *IEEE Transactions on Information Theory*, vol. 52, pp. 1289–1306, Apr. 2006.
- [23] EL-MAHALLAWY, M. and HASHIM, M., "Material classification of underground utilities from GPR images using DCT-based SVM approach," *IEEE Geoscience and Remote Sensing Letters*, vol. 10, pp. 1542–1546, Nov. 2013.
- [24] EL-SHENAWE, M. and RAPPAPORT, C. M., "Monte Carlo simulations for clutter statistics in minefields: AP-mine-like-target buried near a dielectric object beneath 2-D random rough ground surfaces," *IEEE Transactions on Geoscience and Remote Sensing*, vol. 40, pp. 1416–1426, Jun. 2002.
- [25] EMBREE, P., BURG, J., and BACKUS, M., "Wide-band velocity filtering - the pie-slice process," *Geophysics*, vol. 28, no. 6, pp. 948–974, 1963.
- [26] FELSEN, L. B. and MARCUVITZ, N., *Radiation and Scattering of Waves*. Prentice Hall, 1973.
- [27] FENG, X., SATO, M., ZHANG, Y., LIU, C., SHI, F., and ZHAO, Y., "CMP antenna array GPR and signal-to-clutter ratio improvement," *IEEE Geoscience and Remote Sensing Letters*, vol. 6, pp. 23–27, Jan. 2009.

- [28] FIENUP, J. R., “Synthetic-aperture radar autofocus by maximizing sharpness,” *Optics Letters*, vol. 25, no. 4, pp. 221–223, 2000.
- [29] FRENCH, W. S., “Two-dimensional and three-dimensional migration of model-experiment reflection profiles,” *Geophysics*, vol. 39, no. 3, pp. 265–277, 1974.
- [30] GAZDAG, J., “Wave equation migration with the phase-shift method,” *Geophysics*, vol. 43, no. 7, pp. 1342–1351, 1978.
- [31] GIANNOPULOS, A., *GprMax 2.0 (Electromagnetic Simulator for Ground Probing Radar)*, 1988.
- [32] GONZALEZ-HUICI, M. A., “Adaptative stolt migration via contrast maximization for GPR applications,” in *6th International Workshop on Advanced Ground Penetrating Radar (IWAGPR)*, pp. 1–5, 2011.
- [33] GUCUNSKI, N., IMANI, A., ROMERO, F., NAZARIAN, S., YUAN, D., WIGGENHAUSER, H., SHOKOUHI, P., TAFFE, A., and KURAUBES, D., “Nondestructive testing to identify concrete bridge deck deterioration,” Tech. Rep. SHRP2 S2-R06A-RP-1, Transportation Research Board, 2013.
- [34] GURBUZ, A. C., MCCLELLAN, J. H., and SCOTT, W. R., J., “Compressive sensing for subsurface imaging using ground penetrating radar,” *Signal Processing*, vol. 89, no. 10, pp. 1959–1972, 2009.
- [35] GURBUZ, A., MCCLELLAN, J., and SCOTT, W., “A compressive sensing data acquisition and imaging method for stepped frequency GPRs,” *IEEE Transactions on Signal Processing*, vol. 57, pp. 2640–2650, Jul. 2009.
- [36] GÜREL, L. and ÖGÜZ, U., “Transmitter-receiver-transmitter configurations of ground-penetrating radar,” *Radio Science*, vol. 37, no. 3, pp. 5–1–7, 2002.
- [37] GÜREL, L. and ÖGÜZ, U., “Optimization of the transmitter-receiver separation in the ground-penetrating radar,” *IEEE Transactions on Antennas and Propagation*, vol. 51, pp. 362–370, Mar. 2003.
- [38] HATTON, L., LARNER, K., and GIBSON, B., “Migration of seismic data from inhomogeneous media,” *Geophysics*, vol. 46, no. 5, pp. 751–767, 1981.
- [39] HAYASHI, N. and SATO, M., “F-K filter designs to suppress direct waves for bistatic ground penetrating radar,” *IEEE Transactions on Geoscience and Remote Sensing*, vol. 48, pp. 1433–1444, Mar. 2010.
- [40] HUANG, Q., QU, L., WU, B., and FANG, G., “UWB through-wall imaging based on compressive sensing,” *IEEE Transactions on Geoscience and Remote Sensing*, vol. 48, pp. 1408–1415, Mar. 2010.
- [41] HUSRT, M. P. and R., M., “Scattering center analysis via Prony’s method,” *IEEE Transactions on Antennas and Propagation*, vol. AP-35, pp. 986–988, Aug. 1987.

- [42] JAYA, M. S., BOTELHO, M. A., HUBRAL, P., and LIEBHARDT, G., “Remigration of ground-penetrating radar data,” *Journal of Applied Geophysics*, vol. 41, pp. 19–30, Feb. 1999.
- [43] KEE, S. H., TAEKEUN, O., POPOVICS, J. S., ARNDT, R. W., and ZHU, J., “Nondestructive bridge deck testing with air-coupled impact-echo and infrared thermography,” *Journal of Bridge Engineering*, vol. 17, no. 6, pp. 928 – 939, 2012.
- [44] KHAN, U. S. and AL-NUAIMY, W., “Background removal from GPR data using eigenvalues,” in *13th International Conference on Ground Penetrating Radar (ICGPR)*, pp. 1–5, 2010.
- [45] LI, X., LIU, G., and NI, J., “Autofocusing of ISAR images based on entropy minimization,” *IEEE Aerospace and Electronics Systems Magazine*, vol. 35, no. 4, pp. 1240–1252, 1999.
- [46] LOPERA, O., SLOB, E. C., MILISAVLJEVIC, N., and LAMBOT, S., “Filtering soil surface and antenna effects from GPR data to enhance landmine detection,” *IEEE Transactions on Geoscience and Remote Sensing*, vol. 45, no. 3, pp. 707–717, 2007.
- [47] MALLAT, S. G. and ZHANG, Z., “Matching pursuits with time-frequency dictionaries,” *IEEE Transactions on Signal Processing*, vol. 41, pp. 3397–3415, Dec. 1993.
- [48] MARTORELLA, M., BERIZZI, F., and HAYWOOD, B., “Contrast maximization based technique for 2-D ISAR autofocusing,” vol. 152, pp. 253 – 262, 2005.
- [49] MCCLURE, M., QIU, R. C., and CARIN, L., “On the superresolution identification of observables from swept-frequency scattering data,” *IEEE Transactions on Antennas and Propagation*, vol. 45, pp. 631–641, Apr. 1997.
- [50] MORRISON, R. L., DO, M. N., and MUNSON, D. C., “SAR image autofocus by sharpness optimization: A theoretical study,” *IEEE Transactions on Image Processing*, vol. 16, no. 9, pp. 2309–2321, 2007.
- [51] MUKHOPADHYAY, S., WANG, C., BRADSHAW, S., MAXON, S., PATTERSON, M., and ZHANG, F., “Controller performance of marine robots in reminiscent oil surveys,” in *Proceedings of IEEE/RSJ International Conference on Intelligent Robots and Systems*, pp. 1766–1771, 2012.
- [52] MUKHOPADHYAY, S., WANG, C., PATTERSON, M., MALISOFF, M., and ZHANG, F., “Collaborative autonomous surveys in marine environments affected by oil spills,” in *Cooperative Robots and Sensor Networks*, vol. 554 of *Studies in Computational Intelligence*, pp. 87–113, 2014.

- [53] MULLER, R. A. and BUFFINGTON, A., “Real-time correction of atmospherically degraded telescope images through image sharpening,” *Journal of the Optical Society of America*, vol. 64, pp. 1200–1210, 1974.
- [54] NOVAIS, A., COSTA, J., and SCHLEICHER, J., “GPR velocity determination by image-wave remigration,” *Journal of Applied Geophysics*, vol. 65, no. 2, pp. 65–72, 2008.
- [55] NOVO, A., LORENZO, H., RIAL, F. I., and SOLLA, M., “3D GPR in forensics: Finding a clandestine grave in a mountainous environment,” *Forensic Science International*, vol. 204, pp. 134–138, Jan. 2011.
- [56] Ö., Y., *Seismic data Analysis*. Society of Exploration Geophysicists, 2001.
- [57] OLKKONEN, M. K., MIKHNEV, V., and HUUSKONEN-SNICKER, E., “Complex permittivity of concrete in the frequency range 0.8 to 12 Ghz,” in *7th European Conference on Antennas and Propagation (EuCAP)*, pp. 3319–3321, 2013.
- [58] OZDEMIR, C., DEMIRCI, S., and YIGIT, E., “Practical algorithms to focus B-scan GPR images: Theory and application to real data,” *Progress In Electromagnetics Research B*, vol. 6, pp. 109–122, 2008.
- [59] PARRILLO, R., ROBERTS, R., and HAGGAN, A., “Bridge deck condition assessment using ground penetrating radar,” in *European Conference on Non Destructive Testing (ECNDT)*, vol. 103, pp. 1–12, 2006.
- [60] PERSICO, R. and SOLDOVIERI, F., “A microwave tomography approach for a differential configuration in GPR prospecting,” *IEEE Transactions on Antennas and Propagation*, vol. 54, pp. 3541–3548, Nov. 2006.
- [61] RAPPAPORT, C. M., “Accurate determination of underground GPR wavefront and B-scan shape from above-ground point sources,” *IEEE Transactions on Geoscience and Remote Sensing*, vol. 45, no. 8, pp. 2429–2434, 2007.
- [62] SCHNEIDER, W. A., “Integral formulation for migration in two and three dimensions,” *Geophysics*, vol. 43, no. 1, pp. 49–76, 1978.
- [63] SHI, X. and YANG, Q., “Suppressing the direct wave noise in GPR data via the 2-D physical wavelet frame,” in *2011 International Conference on Transportation, Mechanical, and Electrical Engineering (TMEE)*, pp. 1161–1164, 2011.
- [64] SOLDOVIERI, F., BRANCACCIO, A., PRISCO, G., LEONE, G., and PIERRI, R., “A Kirchhoff-based shape reconstruction algorithm for the multimonostatic configuration: The realistic case of buried pipes,” *IEEE Transactions on Geoscience and Remote Sensing*, vol. 46, pp. 3031–3038, Oct. 2008.
- [65] SOLDOVIERI, F., PERSICO, R., and PRISCO, G., “Application of microwave tomography in hydrogeophysics: Some examples,” *Vadose Zone Journal*, vol. 7, pp. 160–170, Feb. 2008.

- [66] SOLDOVIERI, F., PRISCO, G., and PERSICO, R., “A strategy for the determination of the dielectric permittivity of a lossy soil exploiting GPR surface measurements and a cooperative target,” *Journal of Applied Geophysics*, vol. 67, no. 4, pp. 288–295, 2009.
- [67] SOLIMENE, R., CUCCARO, A., AVERSANO, A. D., CATAPANO, I., and SOLDOVIERI, F., “Ground clutter removal in GPR surveys,” *IEEE Journal of Selected Topics in Applied Earth Observations and Remote Sensing*, vol. 7, pp. 792–798, Mar. 2014.
- [68] STOLT, R. H., “Migration by fourier transform,” *Geophysics*, vol. 43, no. 1, pp. 23–48, 1978.
- [69] SUPRAJITNO, M. and GREENHALGH, S. A., “Separation of upgoing and downgoing waves in vertical seismic profiling by contour-slice filtering,” *Geophysics*, vol. 50, no. 6, pp. 950–962, 1985.
- [70] VAN DER MERWE, A. and GUPTA, I. J., “A novel signal processing technique for clutter reduction in GPR measurements of small, shallow land mines,” *IEEE Transactions on Geoscience and Remote Sensing*, vol. 38, pp. 2627–2637, Nov. 2000.
- [71] VAN KEMPEN, L. and SAHLI, H., “Signal processing techniques for clutter parameters estimation and clutter removal in GPR data for landmine detection,” in *Proceedings of the 11th IEEE Signal Processing Workshop on Statistical Signal Processing (SSP)*, pp. 158–161, 2001.
- [72] VUKSANOVIC, B. and BOSTANUDIN, N. J. F., “Clutter removal techniques for GPR images in structure inspection tasks,” *Proceedings of the SPIE on the International Society for Optical Engineering*, vol. 8334, pp. 833413–1–7, Mar. 2012.
- [73] WANG, C., ZHANG, F., and SCHAEFER, D., “Dynamic modeling of an autonomous underwater vehicle,” *Journal of Marine Science and Technology*, in press.
- [74] WANG, J., LIU, X., and ZHOU, Z., “Minimum-entropy phase adjustment for ISAR,” *IEE Proceedings on Radar, Sonar and Navigation*, vol. 151, pp. 203–209, 2004.
- [75] WANG, Y., SHI, Z., WANG, C., and ZHANG, F., “Human-robot mutual trust in (semi)autonomous underwater robots,” in *Cooperative Robots and Sensor Networks*, vol. 554 of *Studies in Computational Intelligence*, pp. 115–137, 2014.
- [76] WANG, Z. W., ZHOU, M., SLABAUGH, G. G., ZHAI, J., and FANG, T., “Automatic detection of bridge deck condition from ground penetrating radar images,” *IEEE Transactions on Automation Science and Engineering*, vol. 8, pp. 633–640, Jul. 2011.

- [77] WEI, X., XIE, Z., and ZHANG, Y., “An investigation on the detectability of deeper rebar layer in concrete bridge decks using GPR,” in *Proceedings of the ASME 2012 Conference on Smart Materials, Adaptive Structures and Intelligent Systems*, p. 8154, 2012.
- [78] WEI, X., XIE, Z., and ZHANG, Y., “Multisensor data fusion and visualization for impact echo testing of bridge decks,” in *Proceedings of SPIE Nondestructive Characterization for Composite Materials, Aerospace Engineering, Civil Infrastructure and Homeland Security*, p. 834707, 2012.
- [79] WEI, X. and ZHANG, Y., “Hyperbolic signature extraction of deeper rebar layer in concrete bridge decks using GPR,” in *Proceedings of the 8th International Workshop on Structural Health Monitoring*, pp. 2578–2585, 2013.
- [80] WEI, X. and ZHANG, Y., “Autofocusing techniques for GPR data from RC bridge decks,” *IEEE Journal of Selected Topics in Applied Earth Observations and Remote Sensing*, in press.
- [81] WEI, X. and ZHANG, Y., “Interference removal for autofocusing of GPR data from RC bridge decks,” *submitted to IEEE Journal of Selected Topics in Applied Earth Observations and Remote Sensing*, revised, 2014.
- [82] WEI, X., ZHANG, Y., and WU, H., “Preliminary study of matching pursuit for extracting GPR rebar reflections,” in *Proceedings of SPIE Nondestructive Characterization for Composite Materials, Aerospace Engineering, Civil Infrastructure and Homeland Security*, p. 86940L, 2013.
- [83] XU, X., MILLER, E. L., and RAPPAPORT, C. M., “Minimum entropy regularization in frequency-wavenumber migration to localize subsurface objects,” *IEEE Transactions on Geoscience and Remote Sensing*, vol. 41, pp. 1804–1812, Aug 2003.
- [84] ZHANG, G., L., T., and KUGA, Y., “Studies of the angular correlation function of scattering by random rough surfaces with and without a buried object,” *IEEE Transactions on Geoscience and Remote Sensing*, vol. 35, pp. 444–453, Mar. 1997.
- [85] ZHANG, Y., WEI, X., TSAI, Y., FETRAT, F., and GUCUNSKI, N., “Multisensor data fusion for impact-echo testing of concrete structures,” *Smart Materials and Structures*, vol. 21, no. 7, p. 075021, 2012.
- [86] ZHAO, W., FORTE, E., PIPAN, M., and TIAN, G., “Ground penetrating radar (GPR) attribute analysis for archaeological prospection,” *Journal of Applied Geophysics*, vol. 97, pp. 107–117, Oct. 2013.
- [87] ZHOU, H., SATO, M., and LIU, H., “Migration velocity analysis and prestack migration of common-transmitter GPR data,” *IEEE Transactions on Geoscience and Remote Sensing*, vol. 43, pp. 86–91, Jan. 2005.

- [88] ZHOU, H., WAN, X., LI, W., and JIANG, Y., “Combining F-K filter with minimum entropy Stolt migration algorithm for subsurface object imaging and background permittivity estimation,” *Procedia Engineering*, vol. 23, pp. 636–641, Mar. 2012.

VITA

Xiangmin Wei was born in 1986 in Jiangsu, China. She received a B.S. degree in Electrical Engineering from Jilin University, Changchun, China, a M.S. degree in Electrical Engineering from Shanghai Jiao Tong University, Shanghai, China, and a M.S. degree in Electrical and Computer Engineering from Georgia Institute of Technology in Atlanta, Georgia, in 2004, 2011, and 2011, respectively. Since the spring of 2011, she has been continuing to pursue the Ph.D. degree in the Electrical and Computer Engineering department of Georgia Institute of Technology in Atlanta, Georgia. Her current research interests are in the areas of sensors (impact echo and ground penetrating radar), signal/image processing for the non-destructive evaluation of concrete structures, and inverse problems of electromagnetic waves.

Publications

- X. Wei, J. Zhou, Y. Zhang, Compressive Sensing for RC Bridge Deck Imaging Using GPR, will be submitted to IEEE Transactions on Geoscience and Remote Sensing in Nov. 2014.
- X. Wei, Y. Zhang, Interference Removal for Autofocusing of GPR Data from RC Bridge Decks, Submitted to IEEE Journal of Selected Topics in Applied Earth Observations and Remote Sensing, 2014, revised.
- X. Wei, Y. Zhang, Autofocusing Techniques for GPR Data from RC Bridge Decks, IEEE Journal of Selected Topics in Applied Earth Observations and Remote Sensing, in press.
- X. Wei, Y. Zhang, Hyperbolic Signature Extraction of Deeper Rebar Layer in

Concrete Bridge Decks using GPR, in Proc. of the 8th International Workshop on Structural Health Monitoring, 2013.

- X. Wei, Y. Zhang, and H. Wu, Preliminary Study of Matching Pursuit for Extracting GPR Rebar Reflections, in Proc. of SPIE Nondestructive Characterization for Composite Materials, Aerospace Engineering, Civil Infrastructure and Homeland Security, 2013.
- X. Wei, Z. Xie, and Y. Zhang, Multisensor Data Fusion and Visualization for Impact Echo Testing of Bridge Decks, in Proc. of SPIE Nondestructive Characterization for Composite Materials, Aerospace Engineering, Civil Infrastructure and Homeland Security, 2012.
- X. Wei, Z. Xie, and Y. Zhang, An Investigation of the Detectability of Deeper Rebar Layer in Concrete Bridge Decks Using GPR, in Proc. of the ASME 2012 Conference on Smart Materials, Adaptive Structures and Intelligent Systems, 2012.
- Y. Zhang, X. Wei, Y. Tsai, J. Zhu, F. Fetrat, and N. Gucunski, Multisensor Data Fusion for Impact-Echo Testing of Concrete Structures, Smart Materials and Structures, vol. 21, no. 7, 2012.
- Z. Xie, X. Wei, and Y. Zhang, Automatic Extraction of Hyperbolic Signatures in Ground Penetrating Radar Images, in Proc. of the ASME 2012 Conference on Smart Materials, Adaptive Structures and Intelligent Systems, 2012.
- Y. Zhang, X. Wei and Z. Xie, "Multisensor Data Fusion for Nondestructive Evaluation of Bridge Decks," in Proc. of SPIE Nondestructive Characterization for Composite Materials, Aerospace Engineering, Civil Infrastructure and Homeland Security, 2011.

- Z. Xie, X. Wei and Y. Zhang, "Impact Echo Signal Interpretation Using Ensemble Empirical Mode Decomposition," in Proc. of the 8th International Workshop on Structural Health Monitoring, 2011.
- Z. Xie, X. Wei, and Y. Zhang, Application of Ensemble Empirical Mode Decomposition in the Impact Echo Test, 8th International Workshop on Structural Health Monitoring, 2011.